Quantum Dots for Intermediate Band in Solar Cells

by

Shadi Dashmiz

A thesis
presented to the University of Waterloo
in fulfillment of the
thesis requirement for the degree of
Master of Applied Science
in
Electrical and Computer Engineering

Waterloo, Ontario, Canada, 2012

I hereby declare that I am the sole author of this thesis. This is a true copy of the thesis, including any required final revisions, as accepted by my examiners.

I understand that my thesis may be made electronically available to the public.

Abstract

The commercially available solar cells suffer from low efficiency and high cost. This would avoid presence of solar cells as a secure energy resource in the market. Problems stem from two facts. Firstly, band gap of materials deployed for cell fabrication do not match the solar spectrum. Secondly, harvesting all the generated electrons is imperfect due to presence of many non-radiative recombination processes and, thermalization of electrons. To transcend these deficiencies, third generation of solar has been introduced. This new generation renders a whole new concept both in design and materials of solar cells scope.

One of new introduction to solar cell field is Quantum Dot (QD). QD offers a broad range of tunability. The optical and electrical properties of QDs can be altered by choice of material, size and shape; therefore; they have great potential for high efficiency cell fabrication. QDs are mainly grown via MBE or synthesized via Colloidal solutions. QDs could be integrated as a part of one of new and promising third generation cells, named Intermediate Band Solar Cells.

QDs could be employed as the intermediate level. If MBE is the selected method for cell fabrication, QDs would grow in a matrix of barrier material accompanied with a wetting layer. Wetting layer would disturb the ideal condition predicted in theory for gaining the high efficiency. To study how wetting layer would affect IB performance two sets of simulations have been carried out. One part is done with COSMOL. In this part different number of QDs layers have been simulated with and without wetting layer. The result showed that parasitic effect of wetting layer could not be eliminated large stacs of QD are stacked together, to achieve the promised efficient wetting layer should be eliminated from the system. In MATLAB part QDs have been approximated with simple cuboid. The main aim in this part was to compare how the result of taking into the account the real shape differs from a simple approach which has been the most reported the most in literature.

If all the restrains on achieving high efficiency of IBSC are met, still one major drawback remains and, that is high cost of MBE process. This would hinder mass production of IB cell. One possible potential method to gradually replace MBE can be Colloidal QDs. Colloidal QDs are fairly low cost and easy to fabricate. In this work, colloidal crystal growth was examined. The best condition for monolayer deposition was obtained and, the feasibility of crystal growth was demonstrated. additionally, There was an attempt to grow more than one layer and investigate result of embedding QDs in a barrier of another

material.

Acknowledgements

I would like to express my sincere gratitude to my supervisor, professor Siva Sivoththaman, for his support, valuable comments, and positive attitude. He has been the source of encouragement for believing in what I am doing.

A special thanks to Dr. Bahareh Sadeghmakki for providing me with keen insight in colloidal QDs field of study. Her help and kindness to me has been really countless.

I also would like to thank all of my colleagues and friends. they have always been very inspiring for me.

Last but not least, special thanks to my dear family for their nonstop love and support. I am incredibly grateful for my wonderful family.

Dedication

This is dedicated to my family.

Table of Contents

List of Figures

Chapter 1

Introduction

1.1 Motivation

Resources of Fossil fuels have been exploited for many decades. They are going to vanish in a near future since the resources are not infinitely available. This fact has resulted in increasing price of fossil fuels. On the other hand, the world's need for energy is increasing. These concerns have obliged governments to investigate for alternative energy resources. One of these promising energy resources is the sun. It is abundant, could be found everywhere in the world, is free and it is renewable. Solar cell is a device which transforms sun energy into electricity and have been studied extensively for its possibility of being a substitute energy resource.

First generation of solar cell started to appear in the market were wafer-based Silicon cell, this first generation was costly and at the same time its efficiency was relatively low. To abate these limitations, Solar cells started to evolve in order to lower the cost and boost the efficiency. The second phase of evolution was named second generation of solar cells. This generation is based on thin film technology and employs different materials. It has broken through the monopoly of Silicon for cell fabrication. This generation although successful to address the issues of first generation, still is far from the desired cost. The desired cost is achieved when the whole fabrication process expenses approaches that of constituent materials. At the same time incrementing efficiency double or triple as what it is available by second generation is the ultimate desire. To make this solar cells technology happen a very mature high-tech fabrication process is required. This mature low-cost high-efficiency solar cell technology is called third generation [6]. A diagram of demonstrating

efficiency and cost of each generation is shown in Fig. 1.1

Highest achieved efficiency up to now is 43.5% [7] using the III-V material, system. It is much higher than the efficiency achievable through conventional Silicon Solar cell. The highest achieved silicon solar cell efficiency is 25% [7] which is not comparable to devices employing new material system. So it is logical to invest more on new material system as well as improving conventional methods to achieve higher efficiency in order to making solar cells competitive to other energy resources. In theory efficiency of solar cell can be close to Carnot limit of 95% if sun is modelled as a black body object at $6000K$ and cell temperature is $300K$. If achieved, this would lead to a revolution of energy access. Third generation of solar cell if achieved would be a prominent step to get close to Carnot limit as shown in Fig. 1.1 [1].The reason behind substantial efficiency increase of third generation solar cells is harvesting more photons which means efficient use of solar spectrum.

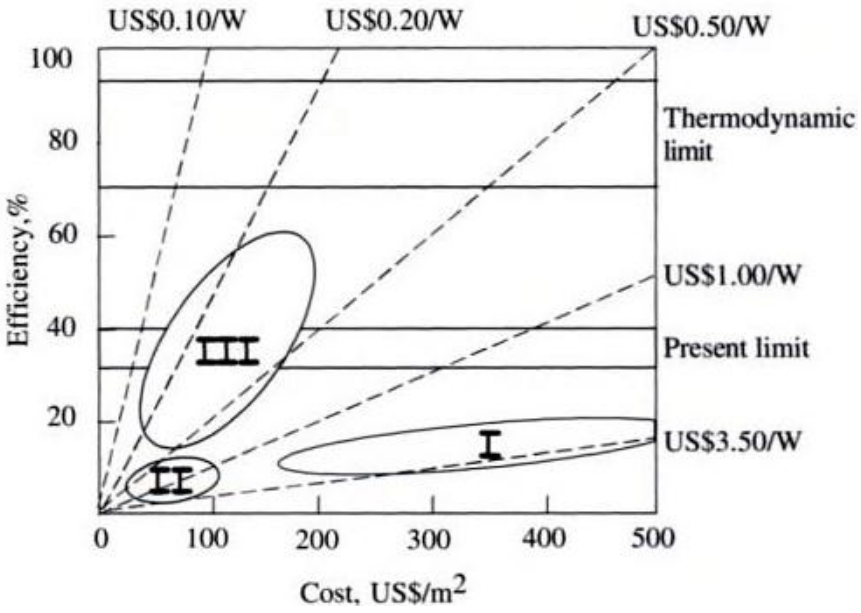

Figure 1.1: Diagram of efficiency VS cost for different solar cells generations[1]

One of third generation solar cell's concepts which has appealed to many researchers is Intermediate Band Solar Cell. This solar cell promises for one of highest efficiencies; however, so far this high efficiency has not been realized. There are several reasons for this failure. Firstly, the proper material suiting the IB requirement has not been completely

developed. Secondly, the device design has not been optimum yet. Thirdly, many different physical phenomena occur in real devices which the theory lacks to take into consideration. Theory holds for ideal condition, however, in experiments many parasitic phenomena interfere with the ideal condition. If all of these limitations are addressed, there is still a major restriction for its mass production and that is the very high cost of its fabrication by MBE method. MBE is a method for QD fabrication and, currently is the principal method for IB fabrication.

1.2 Objective

There are three main objectives in the presented thesis. Firstly, investigating the effect of different number of stacked layers of quantum dots on the intermediate energy level taking into account the realistic shapes of QDs. Secondly, exploring the effect of adding wetting layer on the band formation. Wetting layer is a Quantum Well which forms inevitably during QD growth via MBE method. Wetting layer is one of trouble making elements which would deviate the IBSC form its ideal condition. Thirdly, possibility of colloidal QD crystal formation. Since MBE method is very expensive, alternative fabrication approaches have been intriguing for researchers. One of these approaches could be use of colloidal QD. To accomplish these tasks, for the first two objectives, Matlab and Comsol simulations have been carried out. The main contribution is solving Schrodinger equation for large numbers of stacked QDs layers with the addition of wetting layer and realistic QDs shape consideration. The next step is to examine crystal formation using colloidal QDs In three phases: firstly, likelihood of obtaining Colloidal crystals. Secondly, possibility of embedding quantum dots in a matrix and then, exploring possibility of more than one layer formation in one experiment.

1.3 Thesis Overview

The structure of current thesis is based on 5 chapters. First is the current chapter which is Introduction. The rest of chapters comes as follows:

Chapter 2: this chapter is a comprehensive background on the history of IBSC development, various methods of IBSC fabrication. It also spans basics of quantum dots, their synthesis and growth methods.

Chapter 3: this chapter deals with simulation. Various forms of QDs which are used in IBSC have been simulated. Different numbers of QDs layers have been vertically stacked and simulated in presence and absence of wetting layer. Next part is Matlab simulation. In this part QDs have been approximated with simple cubes and result of this simplistic picture have been compared to the realistic picture of Comsol. At the end of chapter infinite cubic lattice of QDs have been simulated to observe what would be the difference between large number of finite QD layers of real shapes and simple infinite cuboid QDs lattice.

Chapter 4: in this chapter crystal formation using colloidal QDs has been studied since colloidal QDs can serve as a potential replacement for MBE grown QDs. Different conditions for achieving the self-assembly of QDs have been tested.

Chapter 5: this chapter contains conclusion and future work.

Chapter 2

IB cell: an Alternative Solution to Increase Solar Cell Efficiency

2.1 Development of IBSC idea

The photovoltaic effect was first discovered by French physicist A.E. Becquerel in 1839. But, the first solar cell was built in 1883 by Charles Fritts with efficiency around 1%. Since then the solar cell, eventually has developed greatly and, mature industrial solar cells consisting of n and p silicon emitters have been used for many years, in 1961 Shockley and Queisser (SQ) established the efficiency limit of conventional solar cells. They calculated the highest possible efficiency of single junction solar cell to be 40.7% [8].

The main problem here is that this calculation and respective cell just make use of photons with energies higher than band gap. Photons with energies lower than the band gap pass through the cell without being absorbed. Photons with energies higher than the band gap are absorbed but, part of their energy which is the same as band gap is useful for the cell so, part of their energy higher than the band gap is lost via thermalization. This means that the electron which has been transferred from Valence band (VB) to conduction band (CB) loses its additional energy via emitting a phonon instead of emitting a photon as shown in Fig. 2.1.This means that, solar spectrum is just partially absorbed which is the underlying reason for low efficiency of solar cells.

In order to keep solar cell a competitive energy resource in the market, there have been attempts to boost efficiency. So, some innovative approaches have been proposed for

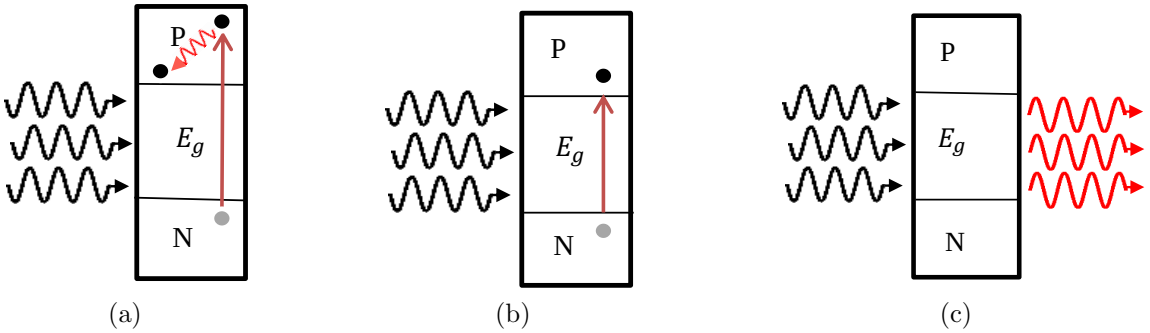

Figure 2.1: (a) photons energy higher than band gap (b) photons energy the same as band gap (c) photons energy lower than band gap

manufacturing high efficiency solar cells capable of exceeding SQ efficiency limit. Some of proposed structures for higher efficiency solar cells are, multi-junction solar cells, hot-carrier solar cells, energy-selective contacts, energy up/down conversion [9], nano-plasmonic structures[10], QD solar cell, multi electron-hole pair generation and intermediate band gap solar cell (IBSc) [11].

Most of these structures focus on three main areas of photon re-utilization. Firstly, harvesting the excess energy of photons with energies higher than the band gap, such as hot carrier solar cells. Secondly, generating more photons and, more electron hole pairs using one photon, such as multiple exciton generations and, up and down conversion. Thirdly, find some solutions to absorb photons with energies lower than the band gap and, adding them to cell current. The latter is the principle idea of IBSC which is shown in Fig. 2.2. If this absorption of lower energy photons could increase the cell output current without degrading the output voltage, the efficiency would be increased drastically.

Wolf was the first who proposed that presence of some energy levels in the mid gap would make the device capable of absorbing lower energy photons [12]. But this method was not successful. Having some energy levels in middle of band gap cannot help pumping electron from valence bands (VB) to intermediate band (IB) and then from IB to conduction band (CB) because these single energy levels act as non-radiative recombination centres due to having localized wave functions as shown in Fig. 2.3.

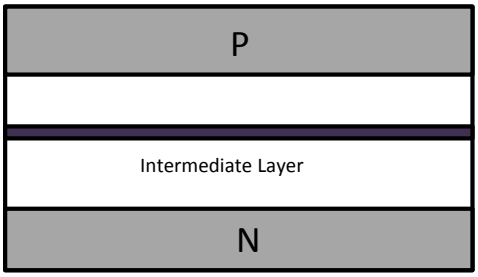

Figure 2.2: Simple illustration of bands in IBSC device

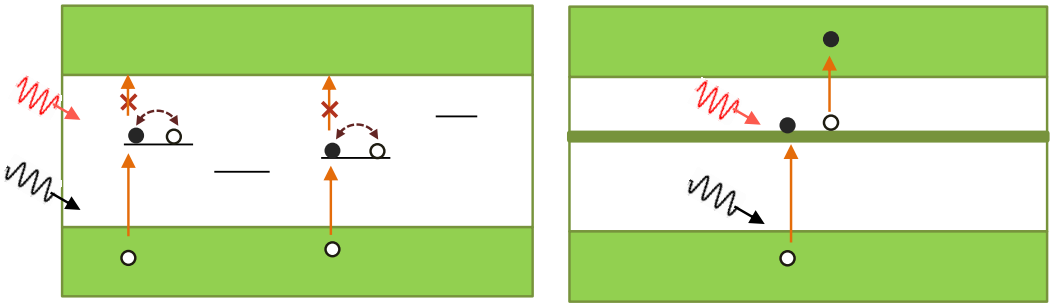

Figure 2.3: comparison between carrier transport single energy levels(a) and a continuous energy level(b)

Although it was an unsuccessful proposal, his idea was the principal of future works for introducing energy bands in the middle of band gap. Based on Wolfs idea, Barnham and Duggan proposed exploiting multiple quantum wells (MQW) in the middle region of GaAs solar cells, for formation of a continues band [13]. This was valuable because it was the first time that nanotechnology was used for manufacturing IB solar cells. However, some controversy had been raised by this proposal, suggesting that MQW method had efficiency the same as single junction conventional solar cell [14, 15]. This efficiency is again limited by detailed balance argument introduced by SQ. The results of researches on MWQ has suggested that any increase in efficiency of MWQ beyond 40.7% , the calculated efficiency for conventional solar cell, would violate the second law of thermodynamics if electron-hole pair is created by absorption of one photon at a time[16].

MWQ idea, although unsuccessful about increasing the efficiency, opened the path for

taking into the account possibility of using nanotechnology for fabrication of intermediate level for absorbing lower energy photons in solar cells.

In 1997, Marti and Luque utilized the detailed balance argument introduced by SQ model with two principals: a) any non-radiative recombination suppressed, b) carriers mobility is infinite and, calculated the efficiency of IBSC shown in Fig. 2.4 to be 63.2% [2, 17].

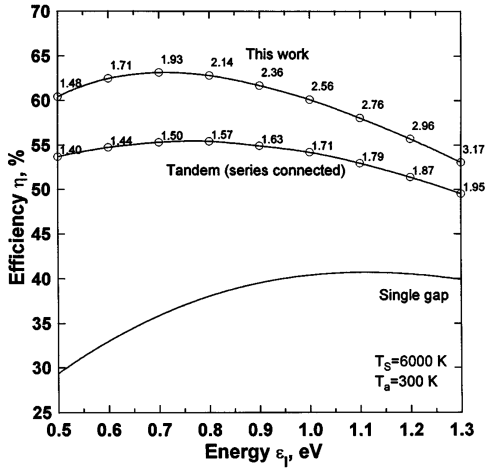

Figure 2.4: Efficiency of IB cell as a function of intermediate band energy level [2]

They measured the optimum band gaps for obtaining this efficiency as follows: $E_{(VB-CB)} = 1.95eV, E_{(CB-IB)} = 0.71eV and E_{(IB-VB)} = 1.24eV$. That was a break-through in solar cell efficiency since there was suddenly an increase from the previous 40.7% efficiency to 63.2%. So, this new method seemed a promising concept for fabricating high-efficiency solar cells.

Since then, there have been efforts to realize this theory and fabricate the device. One of suggested methods as mentioned earlier is use of nanotechnology. The most promising among all methods up to now for fabricating intermediate band has been using Quantum Dots. These structures are attractive because of their ability to form a continues band in the band gap. Also, their zero density of states can provide three separate Fermi levels for IBSC. This is a vital feature for this device. Without this three separate Fermi levels, two of these three energy bands could not exist. Either conduction band or valence band would collapse on intermediate band which in turn would degrade the output voltage because the band gap would reduce to either E_{ci} or E_{iv} which both of them are smaller than E_{cv} as

shown in Fig.2.5; so, efficiency decreases dramatically though current may increase due to reduced band gap.To achieve these separate levels carrier relaxation within each band is assumed to be much faster than the recombination between bands, so that each band has its own Quasi-Fermi level [18, 17].

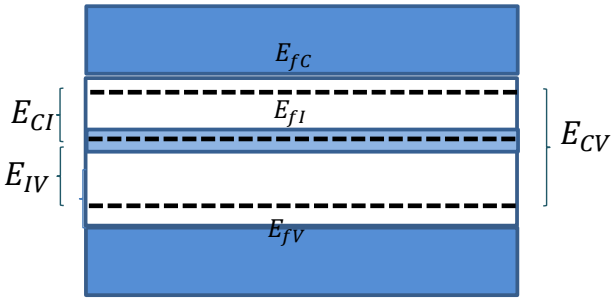

Figure 2.5: Illustration of three separate Fermi levels for IBSC

2.2 Efficiency limit of Intermediate Band Solar Cell

This theory of high efficiency IBSC has been developed based on ideal intermediate band gap solar cell architecture. There are certain ideality rules which govern this detailed balance limit for IBSC, including:

(a) There is no non-radiative recombination between bands.

(b) Carriers have infinite mobilities

(c) No carrier extraction from the intermediate band occurs

(d) Cell can absorb all the photons entering it, meaning that it has enough thickness to do so.

(e) Photons reproduced due to radiative recombination can only escape from the front surface.

(f) There is no overlap between absorption coefficients of three separate bands.

(g) Cell is under isotropic illumination.

The net photo-generated current is proportional to the photon flux between sun and IBSC which is expressed by number of photons leaving the cell. According to above criteria just one band is active for each set of photon energies, assuming that $E_I < E_C$, photon modes leaving the cell are: For $E < E_I$ photons modes escaping from cell are 0; for interval $E_I < E < E_C$ are V_{IV}; for the interval $E_C < E < E_G$ are V_{CI}, and for $E_G < E$ are V_{CV}. Energy levels are shown in Fig. 2.6.

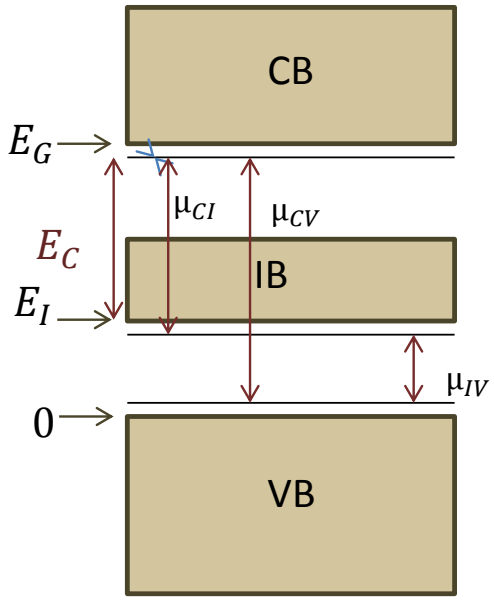

Figure 2.6: Diagram of IBSC energy levels

According to thermodynamic equilibrium distribution of photon flux leaving the cell would be:

$$\dot{N}(\epsilon_m, \epsilon_M, T, \mu) = \frac{2}{h^3 c^2} \int_{\epsilon_m}^{\epsilon_M} \frac{\epsilon^2 d\epsilon}{e^{(\epsilon-\mu)/kT} - 1} \tag{2.1}$$

where ϵ_m and ϵ_M are photon energies, μ is the chemical potential of emitted photon.

So the total current delivered to load is:

$$I/q = [\dot{N}(\epsilon_G, \infty, T_s, 0) - \dot{N}(\epsilon_G, \infty, T_a, \mu_{CV})] + [\dot{N}(\epsilon_C, \epsilon_G, T_s, 0) - \dot{N}(\epsilon_C, \epsilon_G, T_a, \mu_{CI})] \tag{2.2}$$

As it was said there is no current extraction from the intermediate band so:

$$\dot{N}(\epsilon_G, \infty, T_s, 0) - \dot{N}(\epsilon_G, \infty, T_a, \mu_{CV}) = \dot{N}(\epsilon_C, \epsilon_G, T_s, 0) - \dot{N}(\epsilon_C, \epsilon_G, T_a, \mu_{CI}) \tag{2.3}$$

Looking to the Fig. 2.6 the output voltage would be:

$$V = \frac{\mu_C I + \mu_I V = \mu_C V}{q} \tag{2.4}$$

Efficiency is found from these formulas:

$$\omega = \frac{V.I(V)}{Cf\sigma T_s^4} \tag{2.5}$$

$$\eta(x_g, x_c, t_s, f) = I[V(max)]V(max)/P_{inc} = t_s u(x_g) v(f, x_c, x_g) m(v x_g/x_c) \tag{2.6}$$

When efficiency is calculated the highest efficiency is achieved when conduction to valence band bandgap is 1.93 ev, intermediate band to valence band bandgap either 0.7 or 1.23 and intermediate band to conduction band bandgap 1.23 or 0.7 respectively.

2.3 Methods of IBSC fabrication

The main challenge is to realize the additional band in band gap of conventional semiconductors junction. There are different methods to achieve this intermediate band. Some possible approaches are IB bulk materials[19] and, Quantum Dots. The former approach is achieved by engineering the band structure of highly mismatched alloys. A device example is illustrated in Fig.2.7.

As atoms are partially replaced by N atoms to form highly mismatched alloy GaNAs. This alloy possesses another band inherently besides the conduction and valence bands. This additional band which is formed in the band gap of highly mismatched alloy as a result of replacing atoms could be a possible approach for realizing intermediate band solar cell. As the Fig. 2.7 shows the blue line is intermediate band achieved via this design.

Other proposed way of realizing IB is using QDs. QDs could be engineered extensively since choice of their size, shape and materials composition gives a very good degree of freedom for tailoring its properties. Besides, their zero density of states make it possible to form single continuous bands when they are embedded in a host material in large numbers. Most of researches have been focusing on QD IB because of advantages pointed above.

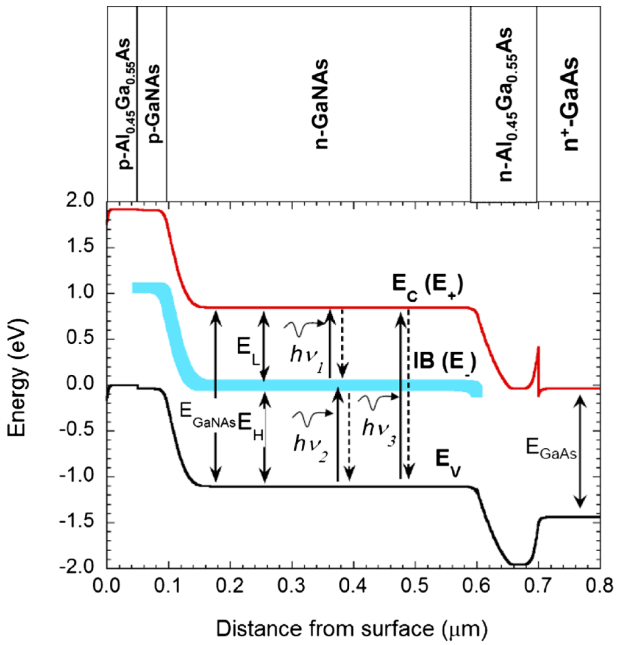

Figure 2.7: Band diagram of IB cell using highly miss matched alloy

2.4 Basics of Quantum Dots

2.4.1 QD Confinement

Quantum dots are three dimensionally confined structures. Meaning that motion of electron inside these structures is limited in all three possible dimensions. Limitation has a quantum meaning. For electron to be confined, the length of allowed movement should be within several De Broglie wavelength of electron wave; otherwise, electron would be regarded as a free particle.

There are different methods to grow QDs. First methods used for QD growth are etching and modulated electric field QD growth. More recent methods of obtaining QDs are self-organized growth [20]and synthesis of colloidal QDs [21, 22]. QDs grown by self -organized method have lens, pyramid, cylindrical and truncated pyramidal shapes. Colloidal QDs could be tailored to be nearly spherical, a faceted sphere though[23, 24]

One main issue in QDs is predicting the band structure and energy levels of one or

more adjacent QDs. Since QDs are 3 dimensional structures,for most of QDs structures a direct solution to Schrodinger equation is not straightforward . Beside that, there are many other effects which make band location of QD to be complicated. So, there have been different simulation approaches proposed to simulate the band structures of QDs.

2.4.2 Schrodinger Equation in a Quantum box

In this structure, finding confined energy levels of a single particle by Schrodinger equation is very simple and solvable as follows[25]:

$$-\frac{\hbar^2}{2m^*}\left(\frac{\partial^2}{\partial x^2}+\frac{\partial^2}{\partial y^2}+\frac{\partial^2}{\partial z^2}\right)\psi(x,y,z)=E_{x,y,z}\psi(x,y,z) \tag{2.7}$$

This equation is valid for the very simple case of having zero potential. This assumption is not valid when taking experimental results into the account. In real world potential is zero inside the QD but is not infinite outside as is the case for the simple cubic box solved here. A material with a finite band gap always exists Outside of QD that would make a none zero potential outside of QD. So, this equation would not be valid and would become more complicated.

By decoupling three-dimensional structure in to 3 one-dimensional equations we would have:

$$-\frac{\hbar^2}{2m^*}\frac{\partial^2}{\partial x^2}\psi(x)=E_x\psi(x) \tag{2.8}$$

$$-\frac{\hbar^2}{2m^*}\frac{\partial^2}{\partial y^2}\psi(y)=E_y\psi(y) \tag{2.9}$$

$$-\frac{\hbar^2}{2m^*}\frac{\partial^2}{\partial z^2}\psi(z)=E_z\psi(z) \tag{2.10}$$

So total energy would be sum of all three decoupled equations which is:

$$E_{x,y,z}=\frac{\hbar^2\pi^2}{2m^*}\left(\frac{n_x^2}{L_x^2}+\frac{n_y^2}{L_y^2}+\frac{n_z^2}{L_z^2}\right) \tag{2.11}$$

This is the simplest form which could be solved analytically. Other important and empirical quantum dot structures are spherical, cylindrical, pyramidal and conical. All other forms do not have a very straightforward analytical solution. Solution to Schrodinger equation of these structures involves using simulation soft wares and numerical methods.

2.4.3 Synthesis of QDs

There are different methods for synthesizing quantum dots. The two main ones are epitaxial self-assembly of QD and, solution based synthesis of colloidal quantum dots. Quantum dots have attracted many researchers due to simplicity of tailoring their properties. For example, quantum dots band gap can be engineered easily which makes them suitable for many photonic and electronics applications such as QD laser[26] or infrared detectors[27].

One of the areas, which has heavily invested on QDs for research is solar cell. Currently there are many ongoing different types of research on how to utilize QDs in solar cells. There are different proposed solar cells structures which employ QDs as part of their design in desire of gaining higher efficiency than the single junction solar cell [28]. One of these research areas is quantum dot intermediate band gap solar cell (IBSC). This structure predicts 63% efficiency which is considerably higher than Shakely-Quassair efficieny limit of 40%.

Once QDs are embedded in another material of different band gap (host), they form heterostructures. If the host material has a greater band gap than QD, a quantum box will form and, carrier confinement occurs. This is due to small available space for electron's movement as shown in Fig. 2.8. Any carrier in the heterostructure either produced thermally or by doping or exists intrinsically tends to lower its energy, therefore, will settle down in the quantum box. Bottom of quantum box CB is lower than that of host material.[25].

There are two different types of heterostructures[29]. Type I and Type II. In type I heterostructures, band offsets are such that conduction band of QD has lower energy than the host material and, valence band of QD has higher energy than the host material. As a result of this both holes and electrons are confined in the QD. This is similar to Fig.2.8 and, is the most studied type of heterostructures. Other type is type II, in this system both of conduction and valence band of QD are either higher than the conduction and valence

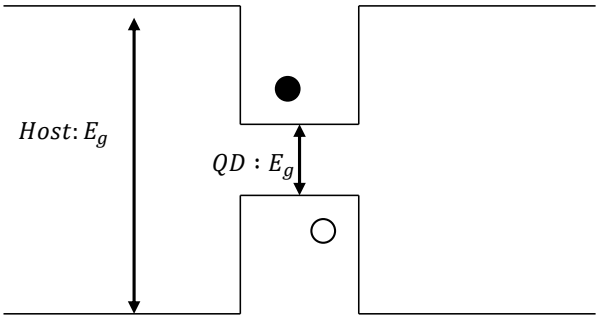

Figure 2.8: Quantum confinement in heterostructures.

band of host material or lower. Such configuration reduces one of carrier confinement. If both QDs conduction and valence bands have lower energy than their host counterpart, electrons will be confined. If both QDs conduction and valence bands have higher energy than host's, holes will be confined. Type II system is shown in Fig. 2.9.

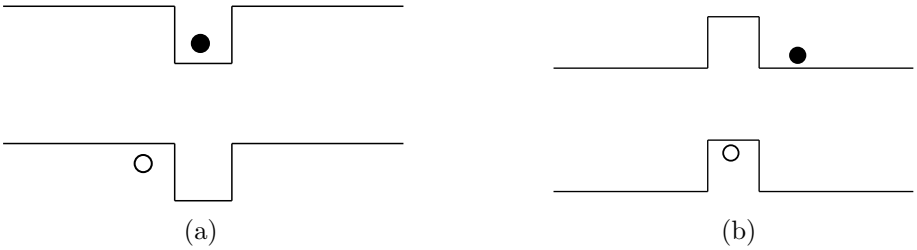

Figure 2.9: Type II heterostructure (a) Electron confinement only(b)Hole confinement only

2.5 Quantum Dot Intermediate Band Solar Cell

A simple conceptual structure of IBSC was illustrated in Fig. 2.2. In that figure quantum dots were sandwiched between two layers of solar cell emitters. It is like filling intrinsic region (i) of a p-i-n solar cell with this quantum dot layers. There are two methods to obtain these quantum dot layers, one is MBE method one potential is colloidal quantum dot crystal growth. Main focus here is MBE method of growing QDs.

2.5.1 Molecular Beam Epitaxy

MBE is used to grow different layers of materials on a substrate epitaxially; it stands for Molecular Beam Epitaxy. Meaning that the layers deposited take the crystalline orientation of their substrate. Species leave the sources and reach to substrate in a beam composed of molecules. Sources are heated if they are solid or liquid to detach molecules from the surface. Since MBE is a line of sight method release of molecules from target could be easily controlled via shutters. Shutters could be open and closed to have a precise control over composition and doping of each layer. Once molecules arrive at the substrate they start to migrate till losing their surface energy and stick to the surface. The deposition rate should be slow enough to ensure molecules have enough time to migrate and lose their energy. Deposition rate of one monolayer per second assures that this condition occurs.

MBE takes advantage of ultrahigh vacuum deposition and, unlike other vacuum deposition methods has a precise control over deposition and growth conditions. Growth conditions and layer composition could be precisely monitored during growth by using reflection high electron diffraction (RHEED), Auger electron spectroscopy (AES) or ellipsometry which lead to eliminating guesswork in MBE [3].Important parts of a MBE machine has shown in Fig. 2.10.

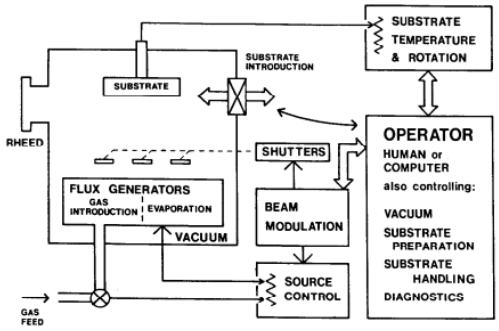

Figure 2.10: Different parts of MBE machine has shown in this figure[3].

MBE deposition is realized with conditions far from thermal equilibrium and growth is governed by surface processes and, kinetics of molecule beam reactions with the outermost layer of substrate. Deposition conditions enable MBE to fabricate very complicated structures. Commonly there are three main modes of crystal growth on a substrate shown in Fig. 2.11[30].

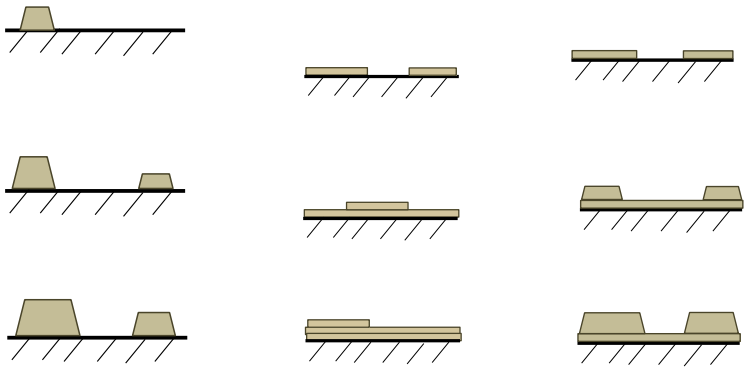

Figure 2.11: three different QD growth modes via MBE (a)Volmer-Weber, island growth(b)Frank-van der Merwe, layer growth(c)Stranski-Krastanov,layer plus island growth

First one is island growth or Volmer-Weber ($V-W$) mode. This happens when deposited atoms or molecules are more strongly bound to each other than they are to the substrate. This causes that they agglomerate together and form islands.

Second mode is layer by layer growth or Frank-van der Merwe ($F-V$). In this mode atoms or molecules have stronger bounding to the substrate than they have to each other. This causes a monolayer of crystalline material being deposited on the substrate. Then another less tight monolayer of material deposits on the previously deposited monolayer and this process continues.

Third mode is Stranski-Krastanov ($S-K$) or layer plus island growth. This is an intermediate stage. After one or several monolayer depositions, monolayer growth will be not favorable anymore due to some system disruption. This reluctancy for further monolayer formation brings about island growth on top of present monolayers. This mode happens when there are two materials with close lattice constants. a brief description this incident is as follows: naming substrate material Y and, deposited molecule material X. It is supposed that surface energy of Y is bigger than X. So, material X would produce a strained monolayer on the substrate. This would decrease the surface energy. The next monolayer deposited on this monolayer of X would have a more reduced surface energy. After several monolayers deposition typically one to three, the surface energy would be succinctly low that new monolayer formation for more reduction of surface energy is not favorable. At

this point, islands of material X would be formed one the previously grown monolayers[31].

2.5.2 MBE Self-Assembled Quantum Dots for IBSC

According to growth modes, two of them create QDs. Stranski-Krastanov and Volmer-Weber. Between these two the former approach is more suitable for most of applications, the latter has fewer applications. This process (S-K) which happens between two lattice-mismatched materials has been the most studied method to develop IBSC devices.

One of material systems which has been studied and well established using MBE deposition is InAs QDs in GaAs matrix. The first experiments for IB cell fabrication have been done by InAs QDs on GaAs substrate[32]. Ten layers of embedded InAs QDs which have a total thickness of 100 nm had been grown as intermediate band. Other experiment for realizing IBSC is deposition of GaSb QDs on GaAs substrate; again ten layers of QDs deposited for IB cell[33]. Several reasons prevent these structures from providing the highest possible efficiency.

One possible reason could be misfit dislocations created during multilayer growth which promotes non-radiative recombination and, disables further QDs layers growth. To overcome this problem one approach is to use material systems with strain symmetries structures like $GaAs_1 - xP_x$ QDs on $In_yGa_1 - yAs$[34].

Other issues could be overlap of absorption coefficients, non-complete coverage of surface by QDs, different non-radiative mechanisms, thermal escape of electrons to CB and non-infinite mobility of carriers are other reasons which lower the efficiency from what is promised by theory of IBSC [17, 35].

One other criteria which is very important for achieving high efficiency of IBSC is optimum placement of intermediate band. According to theory the band placing of all three energy levels of CV, CI and IV are 1.93, 0.7 and 1.23 or 1.93, 1.23 and 0.7 ev respectively. Any deviation from these energy levels would reduce efficiency. Finding materials which could satisfy these band locations is a challenge. Challenge arises from the fact that the energy band of QD IB is not the same as bulk material any more. So, finding the band placing of this layer is not straightforward. Choice of materials, QDs size, distance between QDs layers, QDs shape and quantum effects all have impact on the final band formation.

Since there are several parameters to choose from and, fabrication process is of high cost, it is very important to find the energy bands before any experiments. For this purpose, different simulation techniques have been employed for finding the location of intermediate energy band with different choices of material and QD sizes.

2.6 Potential of Colloidal Quantum Dots for IBSC Fabrication

Another potential approach to fabricate Intermediate band solar cell could be using Colloidal QDs. This method is mainly used for synthesis of II-IV QDs. Colloidal QDs could be synthesized in different solutions such as aqueous and organic. Solution has two main roles. Firstly, is a dispersion medium for nanocrystals and, reactants. Secondly, a place for formation of ligands or surfactants on surface of nanocrystals.

Ligands generally have two different end points, one is a long non-polar alkyl chain and the other one is a polar head. Non polar chains shape and binding strength of polar head affect the synthesis process. Also, ligands stabilize nanocrystals in the solution after their synthesis. The most common types of ligands are tri-n-octylphosphin oxide (TOPO),octadecylamine (ODA). There are various amine and carboxylic acids ligands commonly used as well. Ligands generally burn at 50 C. Growth of colloidal QD has two main parts[4]:
a)Nucleation: for QDs to grow the first step is existence of nucleation sites. Nucleation is governed by Gibbs free energy:

$$\Delta G = \frac{4\pi d_m}{3} r^3 (\mu_c - \mu_s) + 4\pi r^2 \sigma \tag{2.12}$$

There is a critical radius after which crystalline phase growth is possible, this is derived from equation above and shown in Fig. 2.12

b)Cluster growth: creation of small and stable clusters of bound molecules or atoms is the main role of this part. Synthesis is governed by two processes. One, diffusing of particles towards nucleation sites. Two, reaction of particles with the cluster and binding to it. Growth of cluster is demonstrated in Fig. 2.13. The synthesized QD shape is a

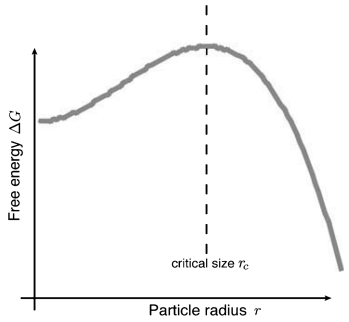

Figure 2.12: Sketch of the potential landscape for the nucleation[4]

faceted spherical.

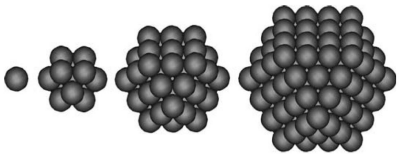

Figure 2.13: Formation of clusters [4]

The cluster is the core of QDs. QDs could be made of pure cores or they could incorporate another material surrounding them named the shell. Shells have superior stability and optical properties compared to core only QDs. Since nanoparticles are very small, they can defuse to human cells. Adding a shell would lower their diffusion ability. Adding a shell would change the QD shape to what is shown in Fig. 2.14[36]. Shell band gap is slightly larger than core for most of popular QD system such as CdSe Core covered with ZnS shell. So the energy band diagram of QD with addition of shell embedded in host material would be Fig. 2.15

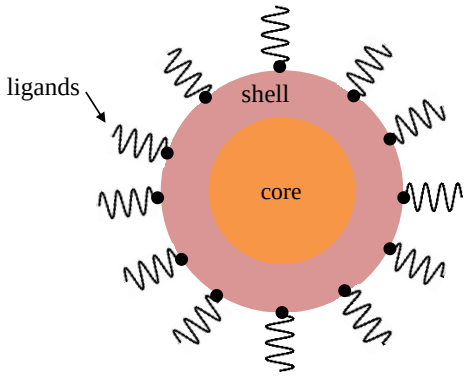

Figure 2.14: A QD consisting of core and shell

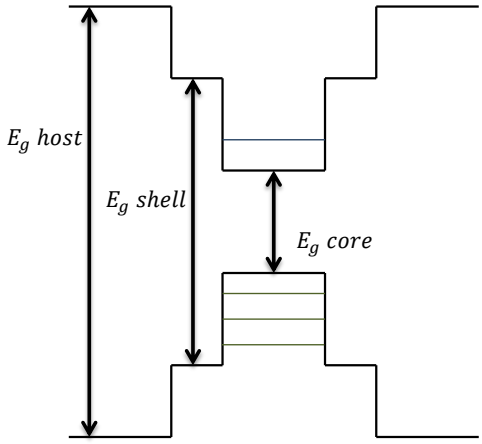

Figure 2.15: Core shell structure's band gap

2.7 Crystal Formation by Colloidal QDs

Once QDs are assembled together they are able form close-packed solids. These structures include glassy Nanocrystal solids with short range order and random orientation and, superlattices which have long range order and desired orientation in 2 and 3 dimensions. The basic short range arrangement of QDs for both glassy and crystalline is shown in Fig. 2.16[5].

Glassy solids form when the force between individual NC is weak or repulsive. When solution is evaporated gradually, space which is available for these NC decreases until the

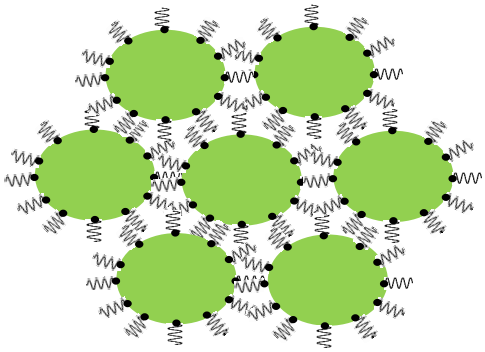

Figure 2.16: Short range arrangement of QDs in both glassy and ordered solids

liquid condenses and freezes, solid is formed when this process ends. By adding the the solvent,This formation is reversible. This solid has short-range order and is similar to an amorphous material as shown in Fig. 2.17.

There are two different type of crystals, faceted colloidal crystal and, ordered thin films. Colloidal crystal is result of homogenous nucleation within the solution and, thin films are result of heterogeneous nucleation at the interface of two materials, one of them is QD itself. The other material could be liquid or solid. Deposition on solid surfaces will produce an ordered crystallite shaped thin film structure while deposition on liquid interface would result in floating ordered island[37].

If there is a very slow process of disturbing QDs in solution while the solvent is evaporating, QDs will have enough time for crystalline arrangements. Having organic stabilizer such as long-tail alkyl and a solution composed of low-boiling alkane and high-boiling alcohol can induce long range order. As solution vaporisers alcoholic part accumulates and slowly causes the QD to separate from dispersed state. Additional force comes from the interaction of polarized metal components of QDs which creates attraction force between QDs to come close together. If the conditions are controlled, time of arriving of separate QDs would be sufficient for finding equilibrium position and at the same time attraction force would remain low to prevent agglomeration.The formation of two colloidal solids are demonstrated in Fig. 2.17[5].

There are many various methods to obtain 3-D crystal of colloidal QDs. The most commons are: Spin cast: one of common methods used for QD thin films. This a very

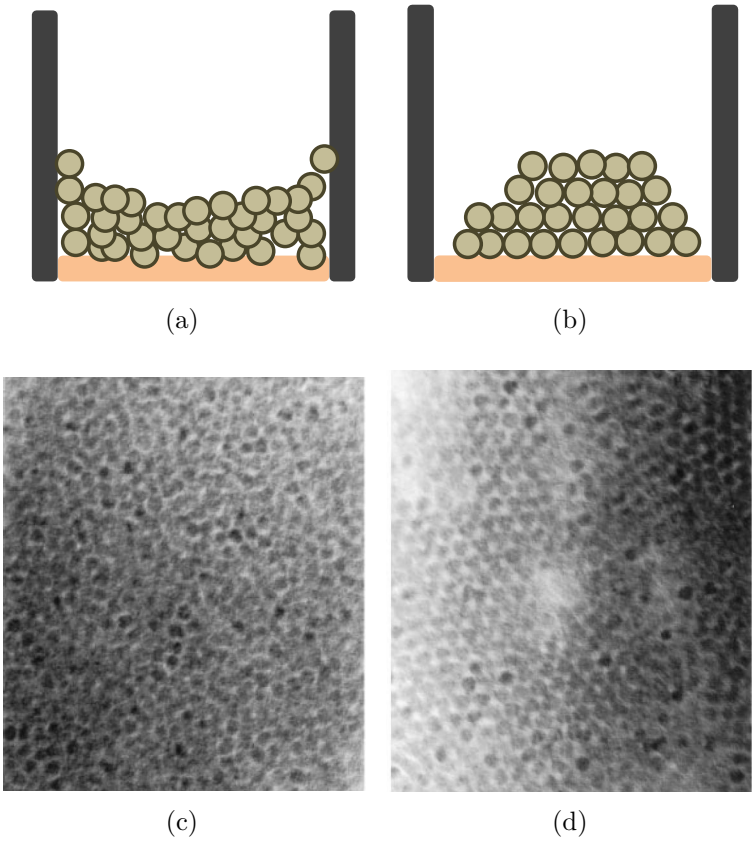

Figure 2.17: two different types of colloidal solids (a)Schematics of crystalline solid formation (b)Schematics of glassy solid formation (c)TEM image a crystalline solid (d)TEM image a glassy solid[5]

simple low cost method but it has the disadvantage that it can produce cracked films[38]. Drop cast: another method of colloidal crystal growth.

Langmuir-Blodgett: an approach of self-assembly by transferring pre-deposited monolayer on the liquid onto a solid substrate. This method deposites a monolayer per cycle.[39].

Dip-coating: another approach of self-assembly is dip-coating. In contrast to previous methods sample enters to the solution vertically[38].

Chapter 3

Comsol and Matlab Simulations of Intermediate Band

There are different ways of simulation QD structures. Most of them employ number of simplifications which would cause deviation of simulation from the real structure. As a result the simulations do not give accurate information about the whole QD structure. So, for example,the band energy extracted from these kinds of very simplified simulation cannot be reliable. There are two more studied ways of simulation of QDs via different software. First approach is to reduce a 3D structure to a 2D one such as reducing QDs to quantum wells and, simulate QW instead of Quantum Dot with some modifications. Simulations of 2D structure could be done easily with different software and they are well established especially if the shape is rectangular, for shapes which are not simple rectangles, simulation becomes more complicated. But the problem is that it is very oversimplified because in most cases shape is not a pure rectangular and approximating QD shape with a rectangle would again give much overlooked information. Other issue is eliminating effect of one confining dimension during 3D to 2D transfer which would reduce the accuracy of result. Another approach is to keep the 3D structure and try to find methods to simulate it in its real shape and structure. There have been several approaches which have attempted to take actual shape and size of Quantum dots into simulation as much as possible. Two main simulation techniques have been employed to simulate QD structures. One of these two principal ideas is finite difference method (FDM). FDM is a numerical method which gives an approximate solution for differential equation through an approximation of derivatives by finite differences. For example to a first order of approximation first derivative of

function f(x) at point a, would be:

$$f'(a) \approx \frac{f(a+h) - f(a)}{h} \tag{3.1}$$

So in the same manner, the Schrodinger equation can be approximated to eliminate derivatives. Then these linear equations are solved in each cell of a rectangular grid taking to account the boundary conditions until the whole grid is solved and then the solution to these linear equations would be final answer for simulation. For 2D structure it is straight forward but, for 3D structures it becomes complicated. This solution is the most common method for simulation of 3D structures using Matlab. The other principal idea of structural simulation is Finite Element Method (FEM). Comsol takes the advantage of using (FEM) instead of FDM. The idea here is the same but with the difference that grid does not have any specific shape. It could be very dense and small wherever is more important or hard to solve. Bigger and sparse wherever it is not a key point in the structure. FEM grid is shown in Fig. 3.1

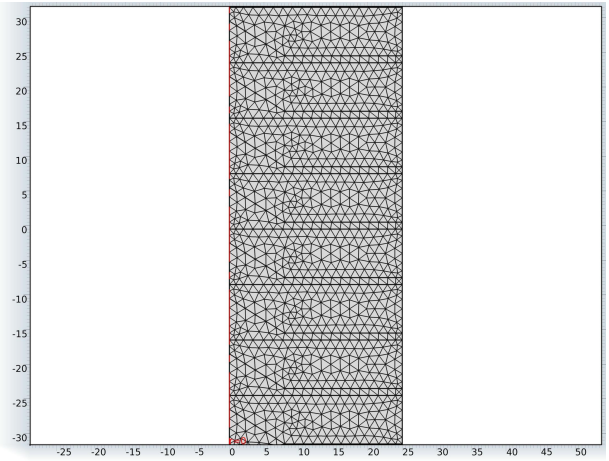

Figure 3.1: FEM grid varies in different parts

So, simulation of 2D and 3D structures would be more accurate especially when the structure is not a very simple shape like most of actual quantum dot structures. Both FDM and FEM solve the linear equation in every single mesh, so the bigger and denser the mesh grid, the more accurate the result will be. Solving a great number of equations requires efficient and fast computers. High requirements of hardware and complication of 3D simulation are the underlying reasons behind reduction a 3D structure to a 2D one. Other problem of most of simulations simulating QD structure for IBSC purpose is the

fact that simulation is done for a quantum dot alone neglecting that in MBE method of growing QDs, particularly in the Stranski-Krastanov growth mode which is the most common method for IBSC fabrication, there is an additional layer which grows inevitably with QD this layer is called wetting layer shown in Fig. 3.2. This thin layer, which is a quantum well attaches to the bottom of QD and, would affect band placing of QDs layers so, should not be ignored [40].

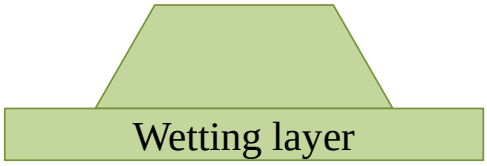

Figure 3.2: Shows how wetting layer becomes an inseparable part of QD

There have been some attempts to take into account the wetting layer during simulation; however, it has been done for a single QD not a complete layer of QDs. Adding this layer would make simulation harder due to having a joint structure which at the same time has two different dimensions, 2D and 3D.

The problem arises when there is need to simulate several layers of QDs together. Finding band placing of an array of QDs is not very straight forward since very large grid is needed which requires to write a very long code and have a very powerful computer to solve a very big matrix of all equation which most of the times normal computers do not have this ability. Problem would be worse when we need to do the simulation for 3D structures like QDs due to having higher number of meshes and 3D matrixes which are not easy to solve, we need to add wetting layer to the system to be as close of possible to real shape of QDs layer for IBSC. This would add more complexity as well.

3.1 A Single Symmetrical QD Formulation

Comsol is able to simulate 3D structure but it requires a huge mesh which most of the times Comsol is not able to produce and simulation could not converge especially if precise meshing is required all over a big structure. This is the case when simulation of arrays of QDs is needed. The solution to this problem is to find a way to transform the QD simulation from 3D to 2D with the minimum deformation of the actual shape. If QD structure

is symmetrical it is possible to transform the 3D structure to 2D with minimum loss of shape; therefore, it is tried to pick the QD structures that are easy to transfer and, at the same time have realistic shapes.

Simulations started with a conical QD with and without wetting layer to investigate the difference in band placing. Conical QD has cylindrical symmetry; therefore; we are capable of reducing the solution from a 3D one to a 2D one. To be able to simulate the structure in Comsol we need to reduce Schrodinger equation from a 3D one to a 2D one as follows [41]:

$$\frac{\hbar^2}{2}\nabla.\left(\frac{1}{m_e(x,y,z)}\nabla\psi(x,y,z)\right)+v(x,y,z)\psi(x,y,z)=E\psi(x,y,z) \tag{3.2}$$

Where h is Plancks constant, is the wave function, E is the eigenvalue (energy), and me is the effective electron mass.

Because of cylindrical symmetry of quantum dots shapes, it is possible to utilize cylindrical coordination instead of Cartesian. Cylindrical symmetry would allow for separation of total wave function to two parts, so a 2D Comsol simulation is possible instead of 3D. This reduction in dimensions is very helpful in terms of mesh gridding and time which takes the model to be solved:

$$-\frac{h^2}{8\pi^2}\nabla.\left(\frac{1}{m_e(r)}\nabla\Psi(r)\right)+v(r)\Psi(r)=E\Psi(r) \tag{3.3}$$

$$\Psi=X(z,r)\Theta(\varphi) \tag{3.4}$$

Inserting the wave function into the Schrodinger equation will result in:

$$-\frac{h^2}{8\pi^2}\left[\frac{\partial}{\partial z}\left(\frac{1}{m_e}\frac{\partial X}{\partial z}\right)+\frac{1}{r}\frac{\partial}{\partial r}\left(\frac{r}{m_e}\frac{\partial X}{\partial r}\right)\right]\Theta-\frac{\hbar^2}{8\pi^2}\frac{X}{m_e r^2}\frac{d^2\Theta}{d\varphi^2}+VX\Theta=EX\Theta \tag{3.5}$$

Dividing the equation by $\frac{X(z,r)}{m_e r^2}\Theta(\varphi)$ and rearranging will result in two sets of separate equations:

$$\frac{1}{\Theta}\frac{d^2\Theta}{d\varphi^2}=-l^2 \tag{3.6}$$

$$-m_e r^2 \frac{h^2}{8\pi^2}\left[\frac{\partial}{\partial z}\left(\frac{1}{m_e}\frac{\partial X_l}{\partial z}\right)\frac{1}{X_l}+\frac{1}{r}\frac{\partial}{\partial r}\left(\frac{r}{m_e}\frac{\partial X_l}{\partial r}\right)\frac{1}{X_l}\right]+m_e r^2[V-E]=-\frac{h^2}{8\pi}l^2 \quad (3.7)$$

Solution to the first part is straightforward and is of the form:

$$\Theta = exp(il\varphi) \quad (3.8)$$

The second equation could be solved using PDE solver of COMSOL after rearranging it as follows:

$$-\frac{h^2}{8\pi^2}\left[\frac{\partial}{\partial z}\left(\frac{1}{m_e}\frac{\partial X_l}{\partial z}\right)+\frac{1}{r}\frac{\partial}{\partial r}\left(\frac{r}{m_e}\frac{\partial X_l}{\partial r}\right)\right]+\left[\frac{h^2}{8\pi^2 m_e}\frac{l^2}{r^2}+V\right]X_l = E_l X_l \quad (3.9)$$

PDE equation general form used in Comsol software is:

$$\nabla.(-c\nabla u-\alpha u+\gamma)+\alpha u+\beta.\nabla u = d_a \lambda u \quad (3.10)$$

By equating two equations, it is easy to find out PDE parameters. Comsol solves equation using Finite Differential Method (FDM) as it was described, and automatically uses more meshes at boundaries and inside the QD than inside the barrier material.

3.2 Simulation Results for Different Stacks of QDs

After transforming 3D structure to 2D, we are going to add more QDs and see the effect of number of QDs on the band formation. Vertical stacks of 60, 120 and 200 QDs have been simulated for this purpose. The same equation has been solved throughout these structures. To make sure that simulation is done properly, it has been checked that Schrodinger equation is solved throughout whole QDs in the vertical stack.

There is a set of boundary conditions which is related to the box in which QD is embedded . As it is shown in the figure 2, for side 1 and 2 zero flux boundary condition has been chosen which lets the wave function to extend to adjacent QDs. Since QDs spread both horizontally and vertically via MBE growth this boundary condition selection allows for a more realistic picture. Especially when taking into account the transportation QDs along the same layer via either tunneling to adjacent horizontal QDs or via delocalization of QD wave function in wetting layer throughout the whole horizontal extension of this

layer. The other two sides boundary conditions has been chosen to be Dirichlet boundary condition which does not let the electron to exit the upper and lower side of box; however, changing of Dirichlet boundary condition to Zero flux doesnt not show significant change in energy levels. 3.3 illustrates a QD/ wetting layer embedded in barrier. Sides 1 and 2 boundary condition lets the electron to transport freely in wetting layer and adjacent QDs.

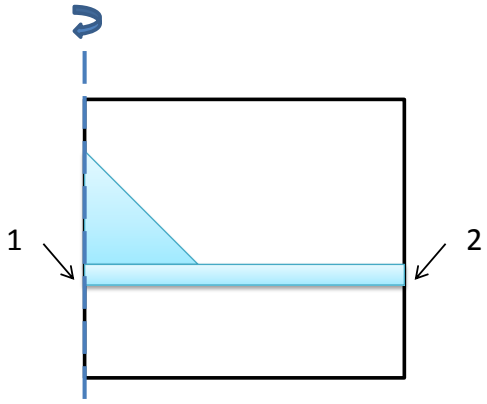

Figure 3.3: Reduction of 3D to 2D because of symmetry. symmetry axis plus side 1 and 2 of boundary conditions are shown in the picture

Experiments have been carried out using l=0 which shows the lowest energy configuration of system, when l is greater than 0 energy levels increase dramatically and for l equals 2 or greater there is no energy level within the QDs, it all spreads out side of QDs to the wetting layer. Fig. 3.4 shows the lowest energy level of truncated conical QD for l=1. The lowest energy level in this mode is higher than the lowest energy level for l=0 by 0.390237 ev.

Material of study is InAs0.9N0.1/GaAs0.98Sb, which has negligible valance band offset and has been proposed to be one of candidate materials for proper position of intermediate band[42].

Dimensions of QDs here are chosen as follows, there are two sizes for each of shapes. One QD of conical and one QD of truncated conical shapes with 2 nm height and base is 8nm (size1), the other two conical QD and truncated conical shapes have 5nm height with base of 16nm (size2). Wetting layer thickness has chosen to be 1nm.

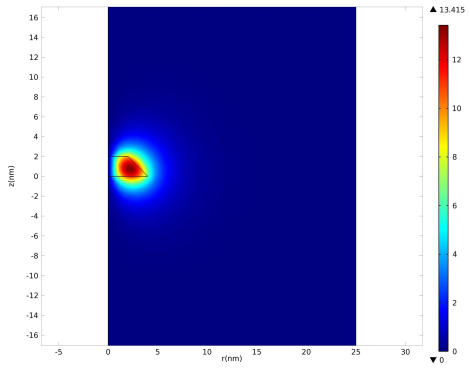

Figure 3.4: As l increases the minimum energy of system increases. figure is for l=1, for l¿1, no energy exists inside QD, (X axis: r(nm), Y axis: z(nm))

To examine how changing the number of aforementioned QD, with and without wetting layer will affect the energy levels, especially what will be the final energy bands resulting from electron resonance in the entire quantum dots, succeeding simulations have been carried out. Firstly, two shapes of QD with the 4 different sizes with and without wetting layer has been simulated. Then, next step was simulating various numbers of vertically stacked QDs from both shapes, resembling the realistic path way of electron along $< 100 >$ direction when the stack is placed in the IBSC device. There are stacks of 60, 120 and 200 QDs with and without wetting layer. The results show how the presence of wetting layer and increasing the number of QDs in a finite array would change the ultimate energy levels. It is assumed that, QDs are sufficiently distanced horizontally to have negligible effect on electron pathway in vertical direction and there is no coupling between two horizontal neighboring QDs. One assumption taken here is that all the QDs in the vertical stack are exactly ordered and, exactly are above one another; however; in reality their placement is a little randomly and, they are not perfectly above one another in the stack. But, for modeling the vertical stack taking this simple picture is feasible[43].

In this part simulations have been done for conduction band only. Holes have heavier effective mass compared to electrons. Higher effective mass of holes causes many bands to exit beside each other. Miniband formation suppresses when many bands are crowded together since no barrier exists to hinder holes movement anymore as shown in Fig. 3.5.

This causes the output voltage to be lower than Eg by valence band offset. For this reason the valence band have not taken into account, presuming that effective band is Eg instead off Eg for all the simulations.

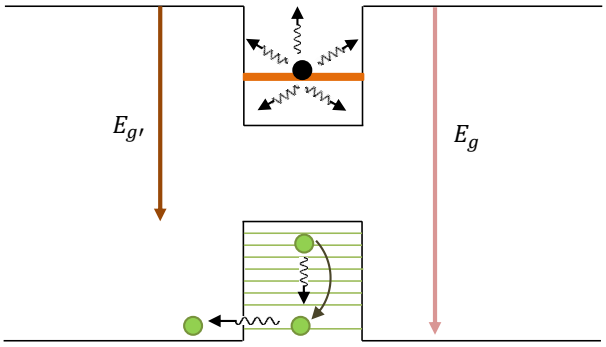

Figure 3.5: Hole energy level VS Electron energy levels

To overcome this voltage reduction, either material systems with negligible valence band offset[44] should be used or the chosen material should possess very low hole effective mass.

3.2.1 Single Quantum Dot

The first sets of simulations for 2 conical QDs and 2 truncated conical QDs are as follows:

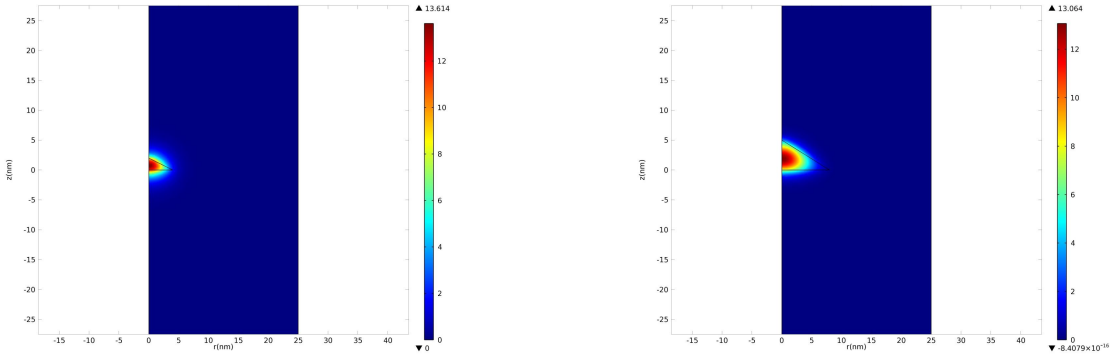

(a) (b)

Figure 3.6: Field distribution for (a) 1 conical QD of size1, energy level shown is 1.04984 ev (b)1 conical QD of size2, energy level shown is 0.4589 ev,(X axis: r(nm), Y axis: z(nm))

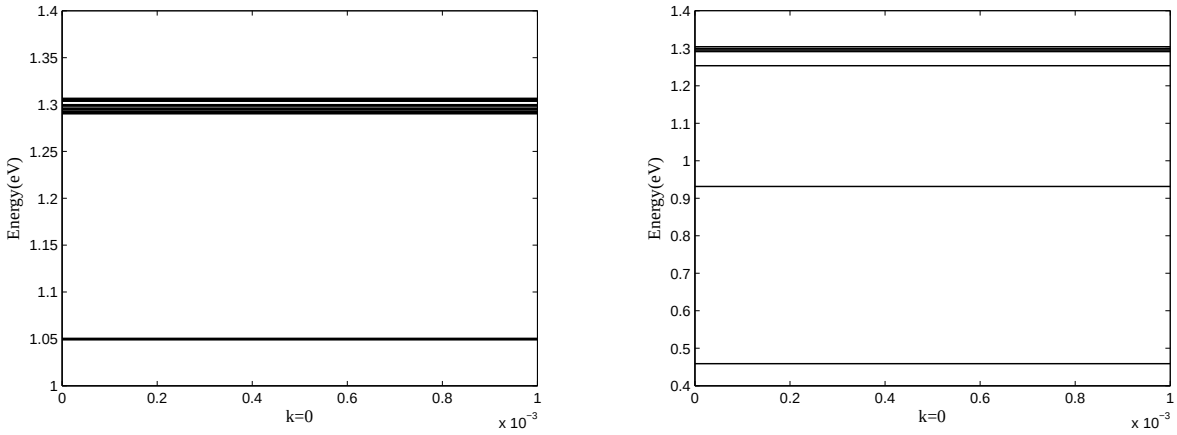

(a) (b)

Figure 3.7: Energy levels of system less than band gap (1.3 ev), for K=0 (a)1 conical QD of size1, (b)1 conical QD of size2)

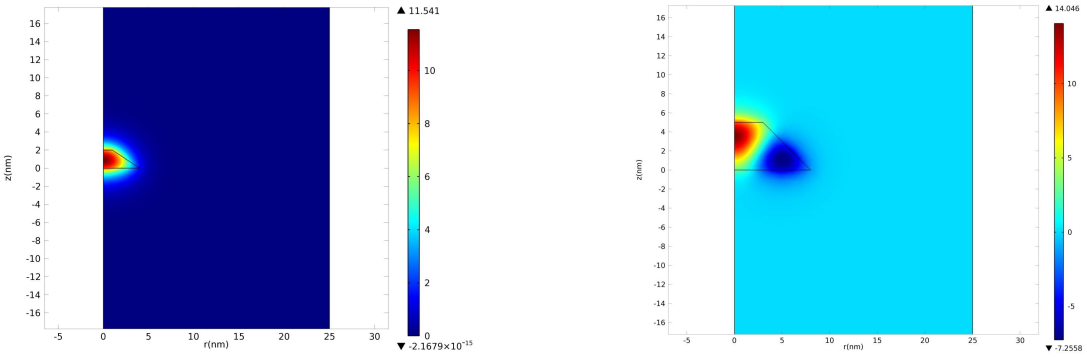

(a) (b)

Figure 3.8: (Field distribution for (a) 1 truncated conical QD of size1 (b)1 truncated conical QD of size2, energy level shown is 0.7879 ev,(X axis: r(nm), Y axis: z(nm))

Comparing figures 3.7 and 3.9, it is understood that increasing size has a very remarkable effect on the energy level placing. Size 2 which has height 5 and base 16 has a very lower energy level compared to the one with height 2 and base 8. For both types of QDs.

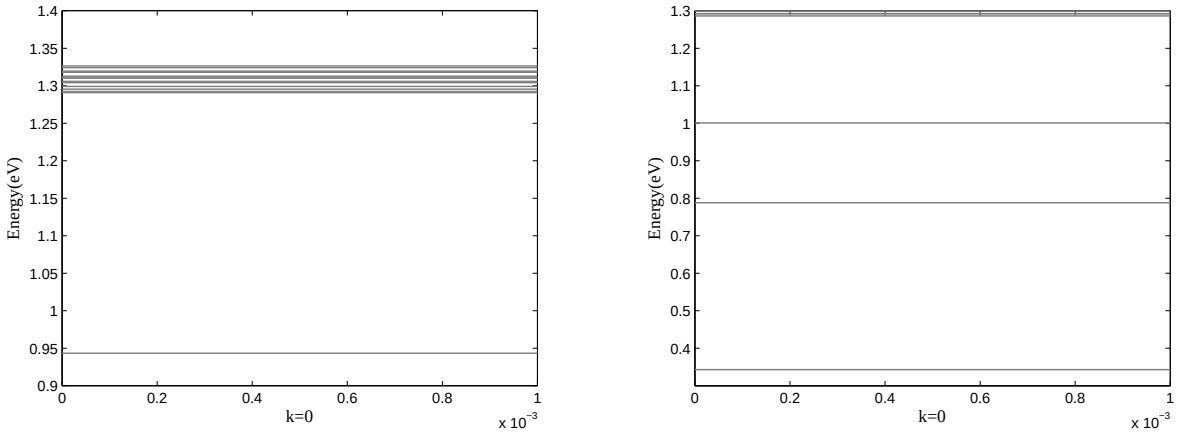

(a) (b)

Figure 3.9: Energy levels of system less than band gap (1.3 ev), for K=0 (a)1 truncated conical QD of size1, (b)1 truncated conical QD of size2)

Comparing conical QDs with truncated ones it would be noticed that for the truncated QD energy levels are a little bit lower for both sizes.

Figure 3.11 and 3.13 show how the energy levels change when wetting layer is added.as it could be seen when wetting layer is added for conical QD of smaller size there is a lot of disturbance around the main energy level and, there exists a continuum of energy levels for smaller QD sizes for both shapes. The situation is the same for conical and truncated conical QDs of bigger size, similarly higher energy levels have been affected and, there is an overall decrease in energy levels compared to the ones without wetting layer.

3.2.2 60 Stacks of Quantum Dots

To see the effect of adding large numbers of QD layers, 60 vertical layers of conical QD and truncated conical QDs with two sizes with and without wetting layer have been simulated. In practice growing large numbers of vertically stacked QDs is not easy due to emitter degradation. Highest number of vertically stacked QDs grown up to now is 50 layers[45]. Although emitter degradation would make large finite arrays of QDs fabrication arduous, most of QD simulation have been done for infinite arrays of QDs. So it is worth to check how large numbers of QDs layers energy bands compares to infinite array energy bands.

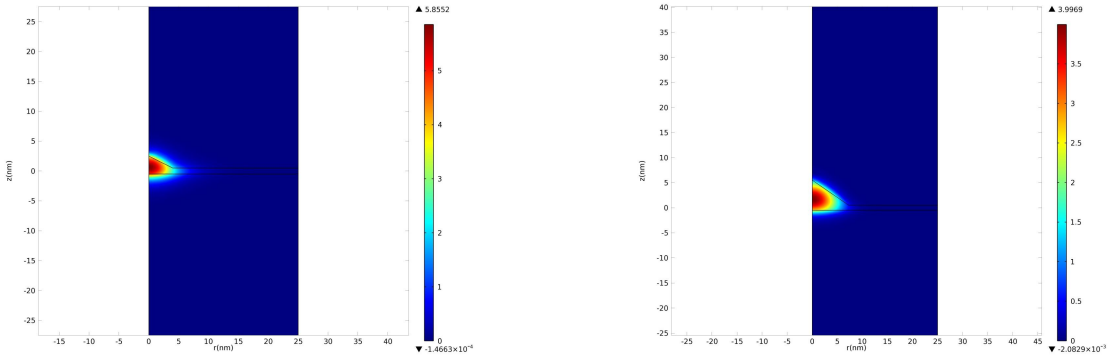

(a) (b)

Figure 3.10: Field distribution for (a) 1 conical QD of size1 plus wetting layer, energy level shown is 0.7805 ev (b)1 conical QD of size2 plus wetting layer, energy level shown is 0.4413 ev,(X axis: r(nm), Y axis: z(nm))

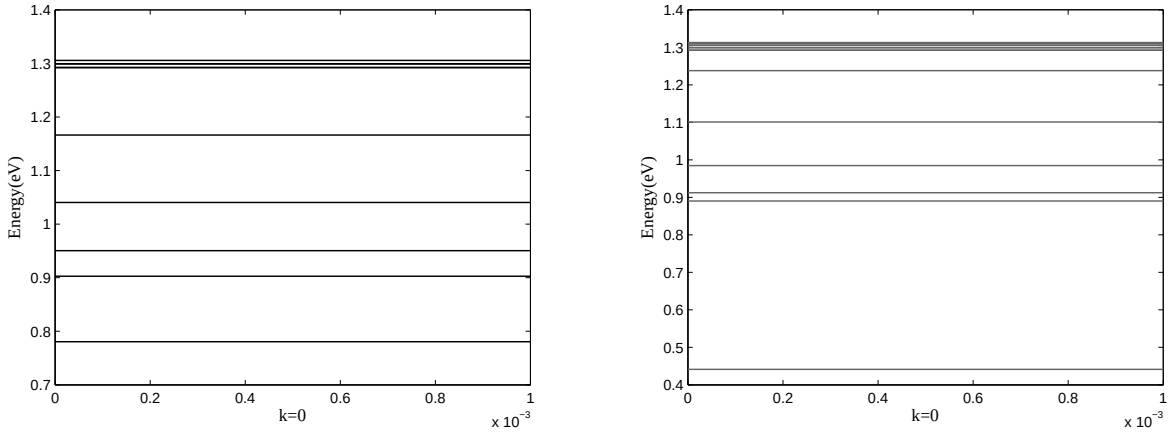

(a) (b)

Figure 3.11: (Energy levels of system less than band gap (1.3 ev), for K=0 (a)1 conical QD of size1 plus wetting layer, (b)1 conical QD of size2 plus wetting layer)

As figure 3.15 and 3.17 show, for conical QD of smaller size, size1, there is one mini-

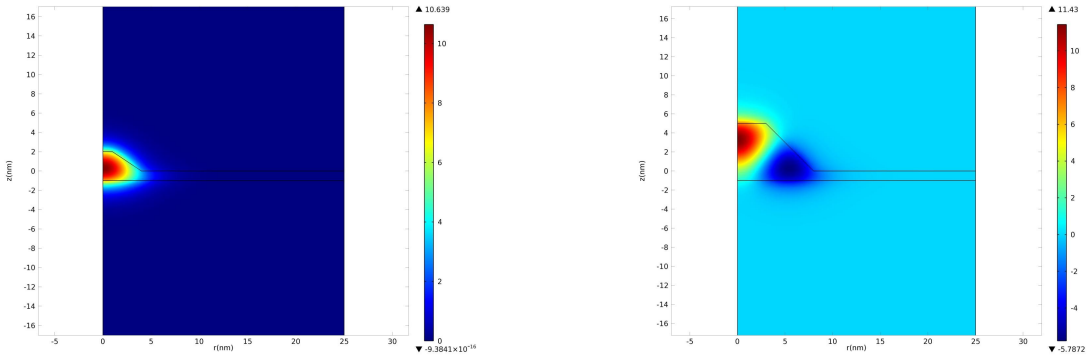

(a) (b)

Figure 3.12: Field distribution for (a) 1 truncated conical QD of size1 plus wetting layer, energy level shown is 0.6779 ev (b)1 truncated conical QD of size2 plus wetting layer, energy level shown is 0.6449 ev,(X axis: r(nm), Y axis: z(nm))

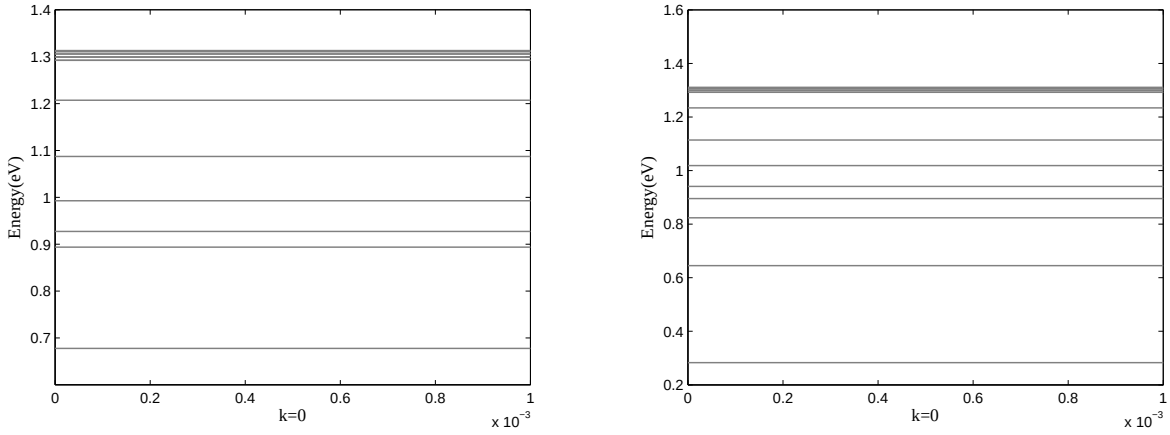

(a) (b)

Figure 3.13: Energy levels of system less than band gap (1.3 ev) for K=0 (a)1 truncated conical QD of size1 plus wetting layer, (b)1 truncated conical QD of size2 plus wetting layer)

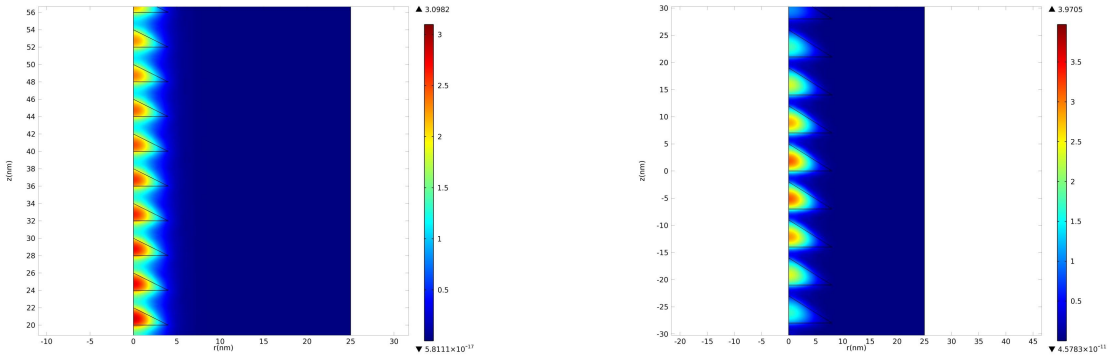

(a) (b)

Figure 3.14: Field distribution for (a) 60 conical QD of size1, energy level shown is 0.9862 ev (b)60 conical QD of size2, energy level shown is 0.4551 ev,(X axis: r(nm), Y axis: z(nm))

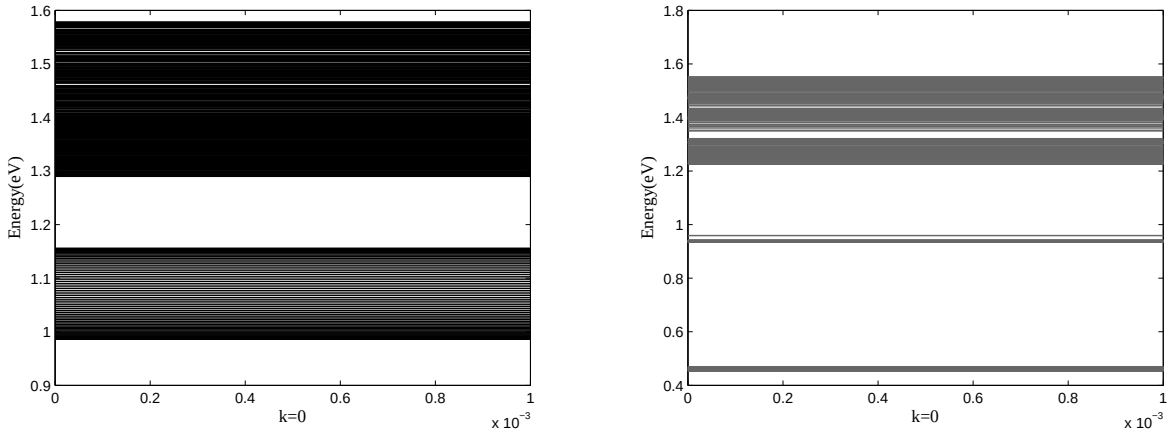

(a) (b)

Figure 3.15: Energy levels of system less than band gap (1.3 ev), for K=0 (a)60 conical QD of size1, (b)60 conical QD of size2)

band around the energy level of the single QD and, is broadened about 0.15 eV. There is also a continuous band at the top of band gap starting from 1.3 ev. The same miniband formation occurs for truncate QD of same size. For QDs of size 2 for both shapes there

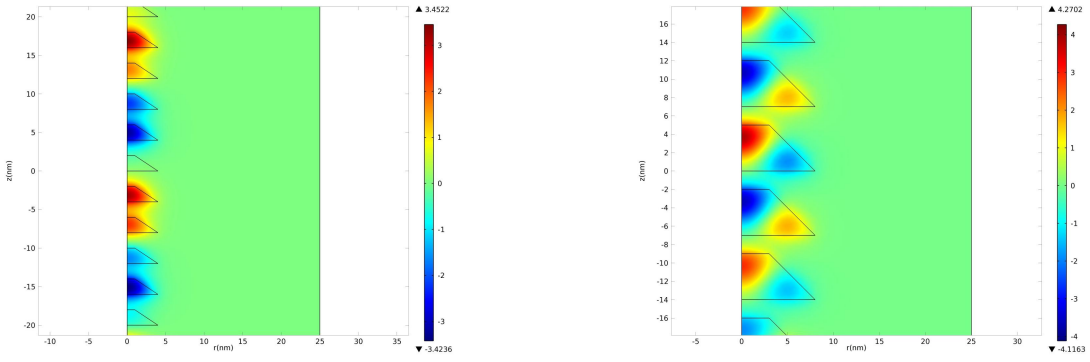

(a) (b)

Figure 3.16: Field distribution for (a) 60 truncated conical QD of size1, energy level shown is 0.9991 ev (b)60 truncated conical QD of size2, energy level shown is 0.7839 ev,(X axis: r(nm), Y axis: z(nm))

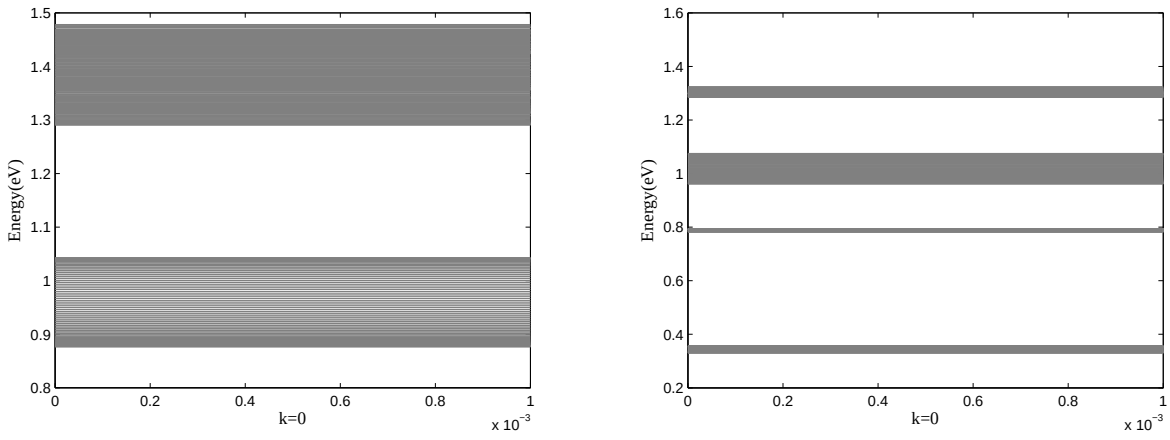

(a) (b)

Figure 3.17: Energy levels of system less than band gap (1.3 ev), for K=0 (a)60 truncated conical QD of size1, (b)60 truncated conical QD of size2)

is not much difference between energy bands of 60 arrays and a single one. Energy bands which are above band gap are a little distinct between 60 arrays and single QD but, are

not of importance for IBSC device.

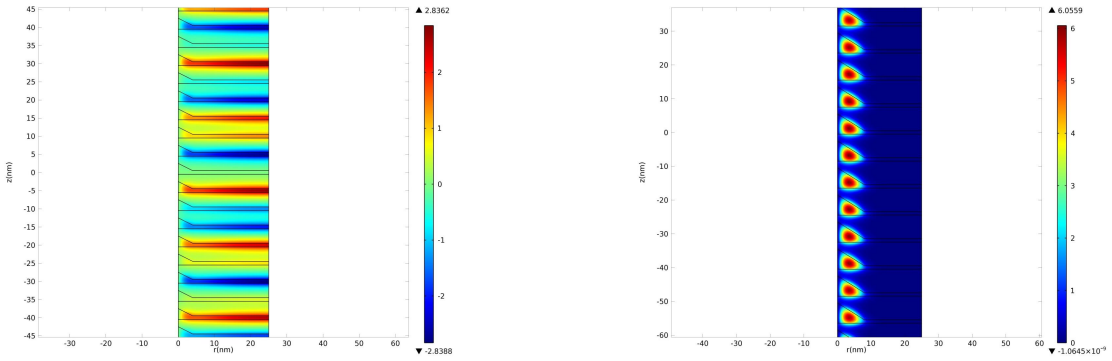

(a) (b)

Figure 3.18: Field distribution for (a) 60 conical QD of size1 plus wetting layer, energy level shown is 0.9027 ev (b)60 conical QD of size2 plus wetting layer, energy level shown is 0.5475 ev,(X axis: r(nm), Y axis: z(nm))

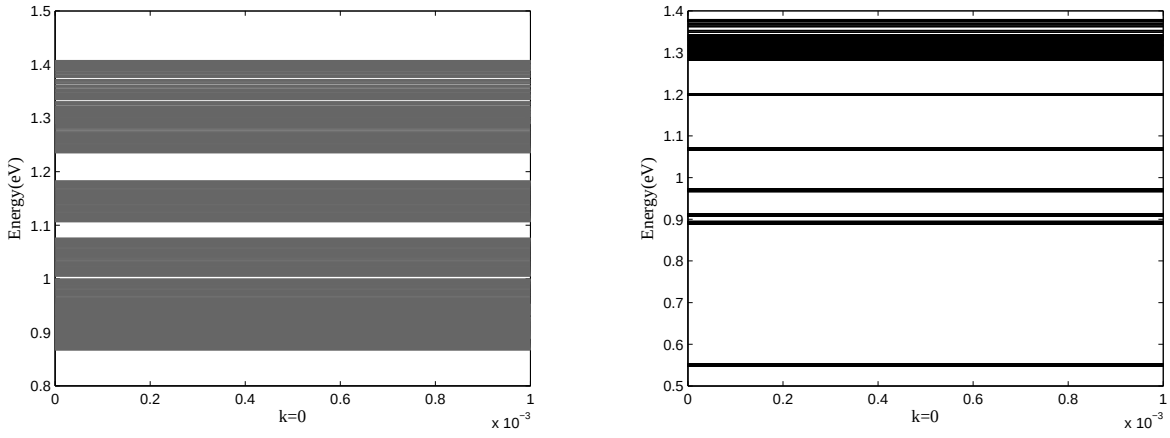

(a) (b)

Figure 3.19: Energy levels of system less than band gap (1.3 ev), for K=0 (a)60 conical QD of size1 plus wetting layer, (b)60 conical QD of size2 plus wetting layer)

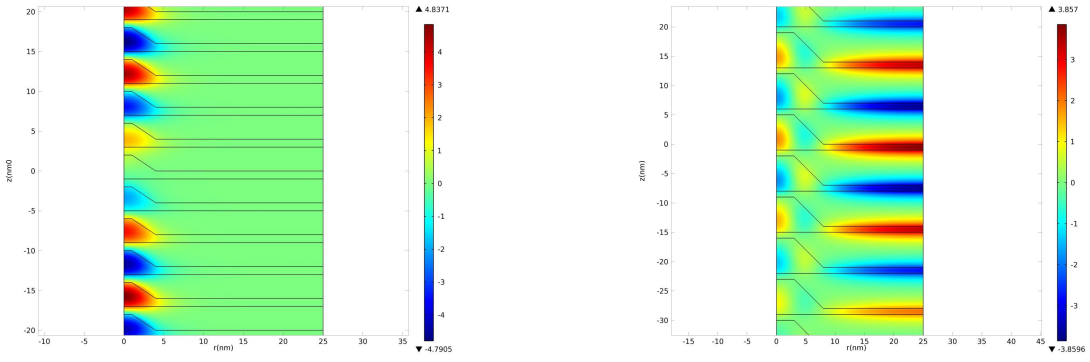

(a) (b)

Figure 3.20: Field distribution for (a) 60 truncated conical QD of size1 plus wetting layer, energy level shown is 0.7863 ev (b)60 truncated conical QD of size2 plus wetting layer, energy level shown is 0.9011 ev,(X axis: r(nm), Y axis: z(nm))

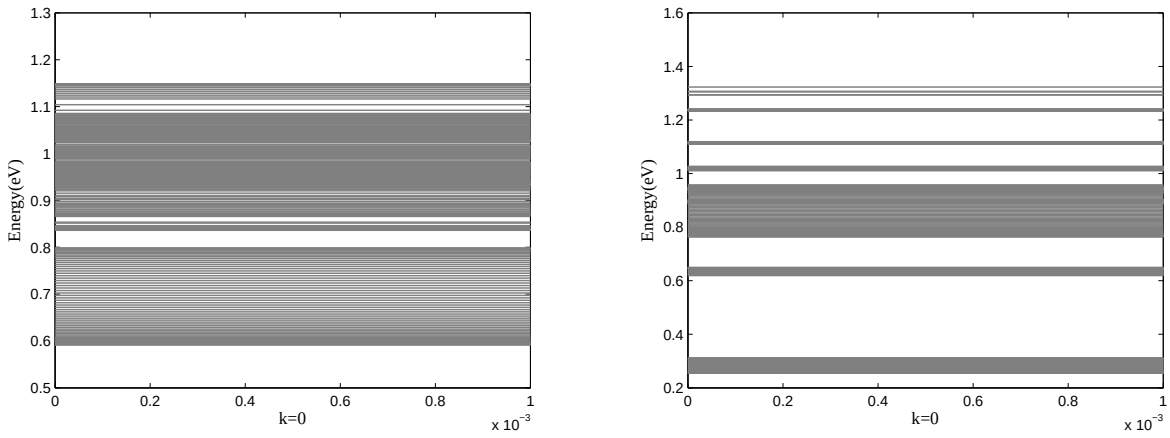

(a) (b)

Figure 3.21: Energy levels of system less than band gap (1.3 ev), for K=0 (a)60 truncated conical QD of size1 plus wetting layer, (b)60 truncated conical QD of size2 plus wetting layer)

Figures 3.19 and 3.21 show energy levels as a function of vertical electron pathway for 60 stacks of 2 QD sizes with different shapes. Adding wetting layer to smaller size QDs would destruct the previous minelayer formation. As it is observed in figures 3.19 and 3.21, energy bands are densely packed together almost connecting bottom of conduction band to the top of conduction band. This is totally undesired for IBSC operation. For larger conical QD however the narrow 0.4 ev and 0.9 ev previously formed bands exist. The main energy levels have not been affected with the presence of wetting layer very explicitly. For truncated conical of size 2, the two lowest consecutive bands have got closer and also have shrunk. For 60 stacks without wetting layer they are 0.4 and 0.8 ev approximately but, for the 60 stack with wetting layer they are around 0.3 and 0.6 ev.

3.2.3 120 Stacks of Quantum Dots

So increasing QDs number even to 60 does not help to have an energy band for smaller QDs shapes. To explore whether increasing number of layers further more would improve band formation at the presence of wetting layer and to check whether energy levels for larger QDs are going to get closer or not, 120 layers of vertically stacked QDs of both sizes and shapes have been simulated. Again with presence and absence of wetting layer.

Result of simulations for conical and truncated conical of size 1 and 2 does not differ from the previous 60 stacks. As illustrated in figures 3.23 and 3.25. This means that if wetting layer is not present a mini band would form inside the band gap of small QDs. Band engineering would permit for selective placing of miniband. Also, the same happens for larger QD size. Energy levels are almost unchanged; therefore, band engineering would transform energy levels to the desired levels.

This time wetting layer has been added to 120 layers of vertically stacked QDs for both sizes and shapes. As figures 3.27 and 3.29 demonstrate, For smaller QDs, the miniband degrades completely and, for larger dots lower energy levels remained almost unchanged. For QDs of size 2 higher energy levels are affected with wetting layer presence.

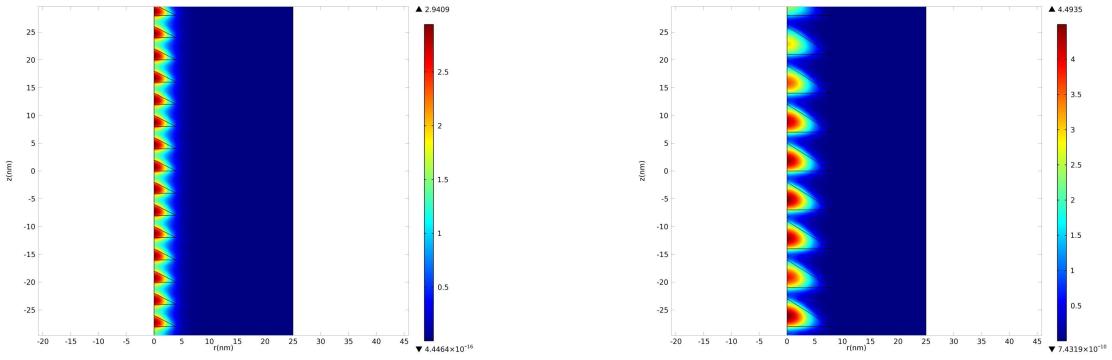

(a) (b)

Figure 3.22: Field distribution for (a) 120 conical QD of size1, energy level shown is 0.9859 ev (b)120 conical QD of size2, energy level shown is 0.4550 ev,(X axis: r(nm), Y axis: z(nm))

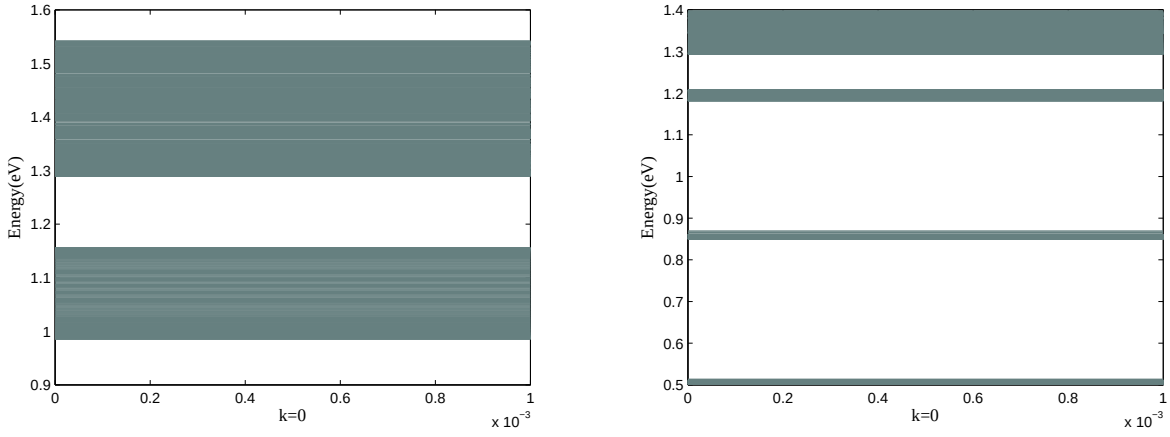

(a) (b)

Figure 3.23: Energy levels of system less than band gap (1.3 ev), for K=0 (a)120 conical QD of size1, (b)120 conical QD of size2)

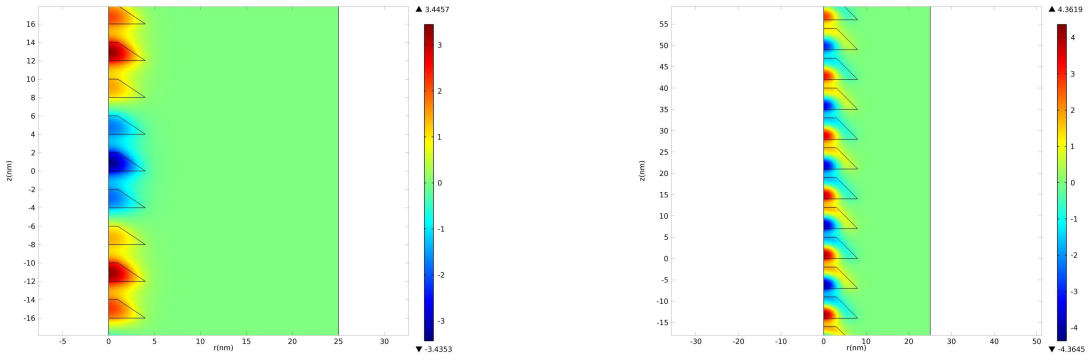

(a) (b)

Figure 3.24: Field distribution for (a) 120 truncated conical QD of size1, energy level shown is 0.9067 ev (b)120 truncated conical QD of size2, energy level shown is 0.9626 ev,(X axis: r(nm), Y axis: z(nm))

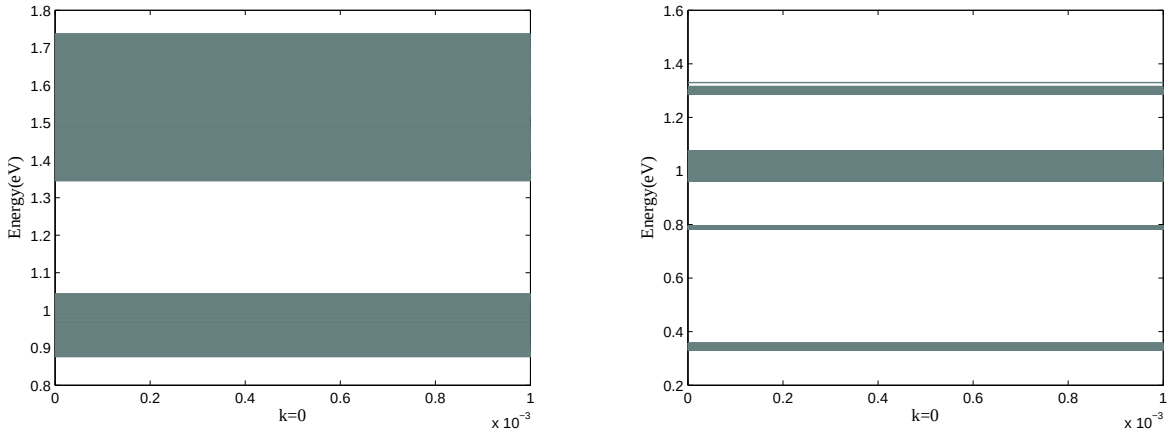

(a) (b)

Figure 3.25: Energy levels of system less than band gap (1.3 ev), for K=0 (a)120 truncated conical QD of size1, (b)120 truncated conical QD of size2)

3.2.4 200 Stacks of Quantum Dots

The last part is simulating the same structures this time with 200 stacks. Since this number is so large compared to the technology of experimental fabrication so far, this would

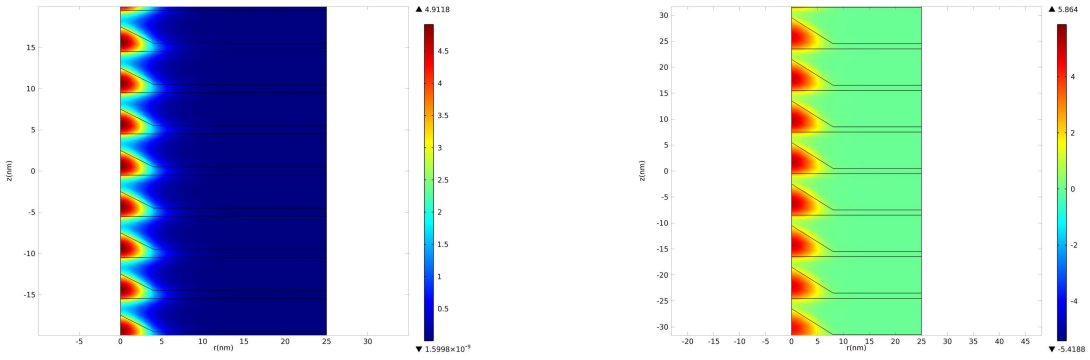

(a) (b)

Figure 3.26: Field distribution for (a) 120 conical QD of size1 plus wetting layer, energy level shown is 0.7029 ev (b)120 conical QD of size2 plus wetting layer, energy level shown is 0.3580 ev,(X axis: r(nm), Y axis: z(nm))

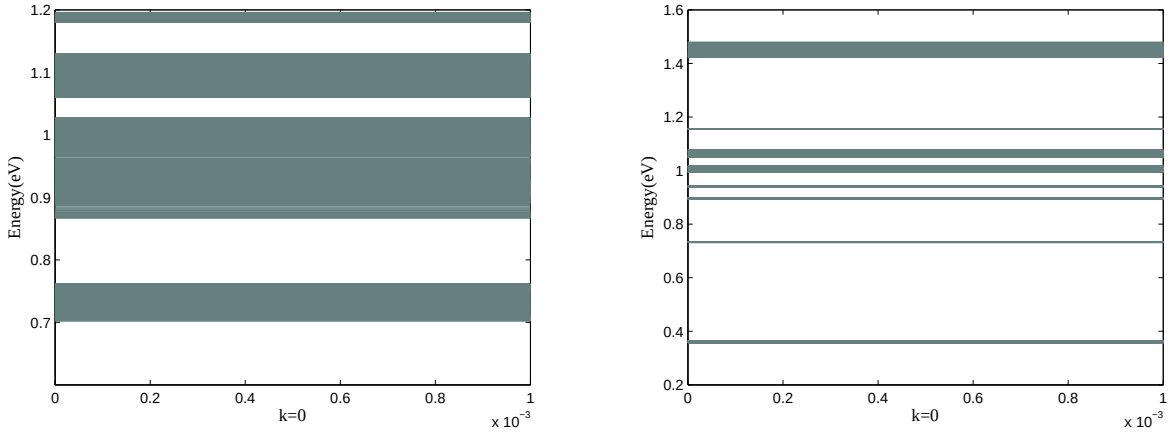

(a) (b)

Figure 3.27: Energy levels of system less than band gap (1.3 ev), for K=0 (a)120 conical QD of size1 plus wetting layer, (b)120 conical QD of size2 plus wetting layer)

be regarded as an infinite array. This is the last comparison between different sizes and the two structures. This has been done to make sure that increasing number of QDs layer

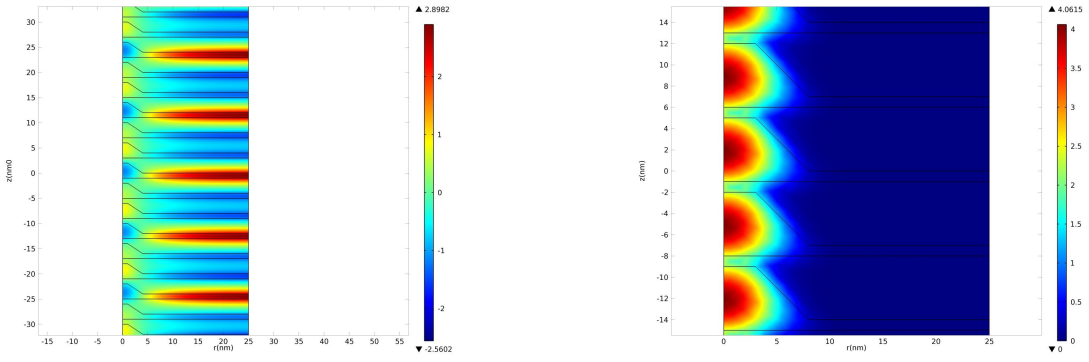

(a) (b)

Figure 3.28: Field distribution for (a) 120 truncated conical QD of size1 plus wetting layer, energy level shown is 0.9341 ev (b)120 truncated conical QD of size2 plus wetting layer, energy level shown is 0.2546 ev,(X axis: r(nm), Y axis: z(nm))

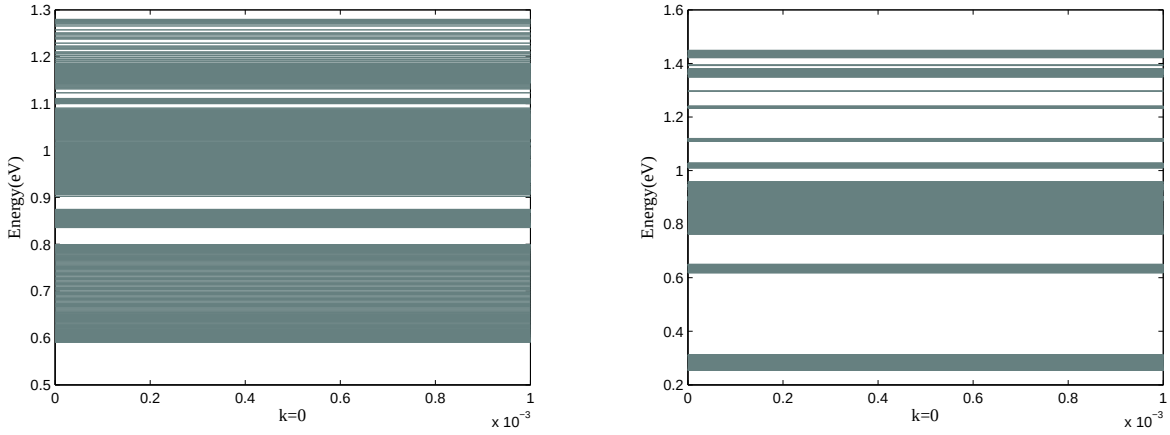

(a) (b)

Figure 3.29: Energy levels of system less than band gap (1.3 ev), for K=0 (a)120 truncated conical QD of size1 plus wetting layer, (b)120 truncated conical QD of size2 plus wetting layer)

would not compensate for the detrimental effect of wetting layer.

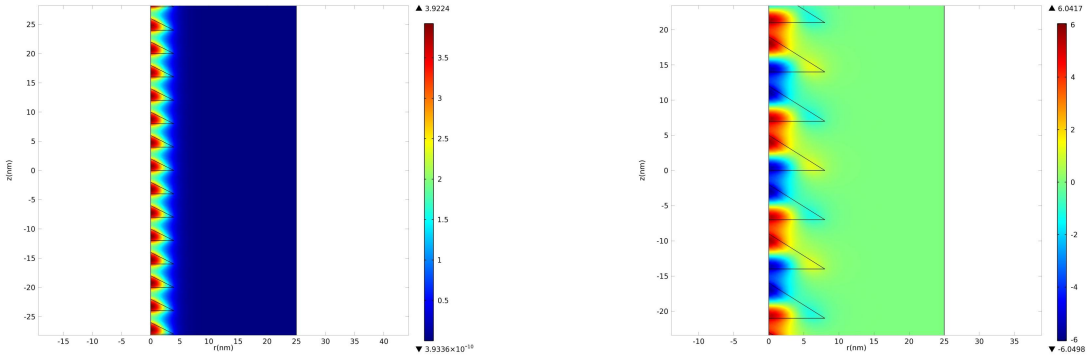

(a) (b)

Figure 3.30: Field distribution for (a) 200 conical QD of size1, energy level shown is 0.9851 ev (b)200 conical QD of size2, energy level shown is 0.2297 ev,(X axis: r(nm), Y axis: z(nm))

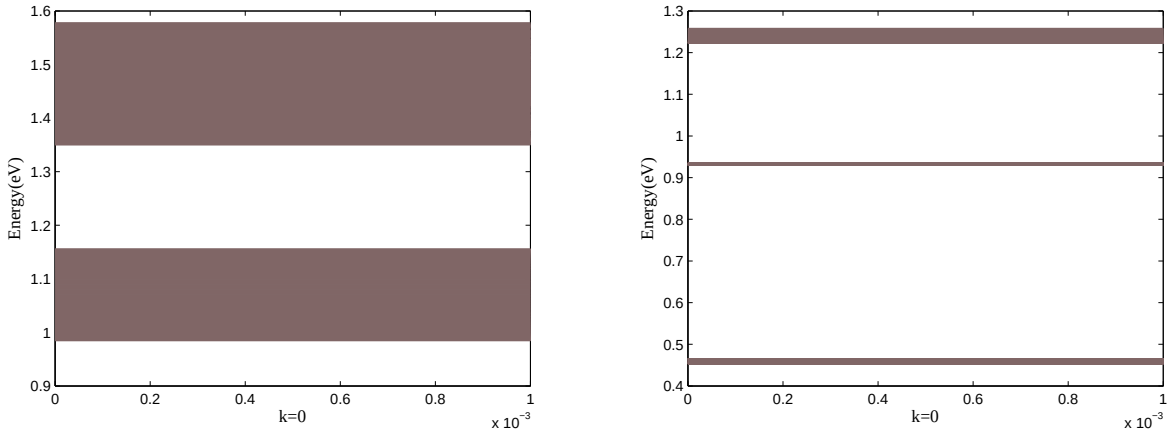

(a) (b)

Figure 3.31: Energy levels of system less than band gap (1.3 ev), for K=0 (a)200 conical QD of size1, (b)200 conical QD of size2)

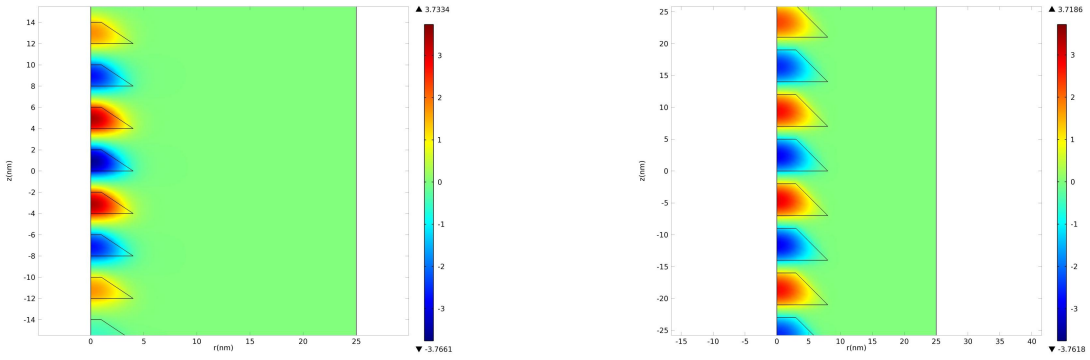

(a) (b)

Figure 3.32: Field distribution for (a) 200 truncated conical QD of size1, energy level shown is 1.0353 ev (b)200 truncated conical QD of size2, energy level shown is 0.3557 ev,(X axis: r(nm), Y axis: z(nm))

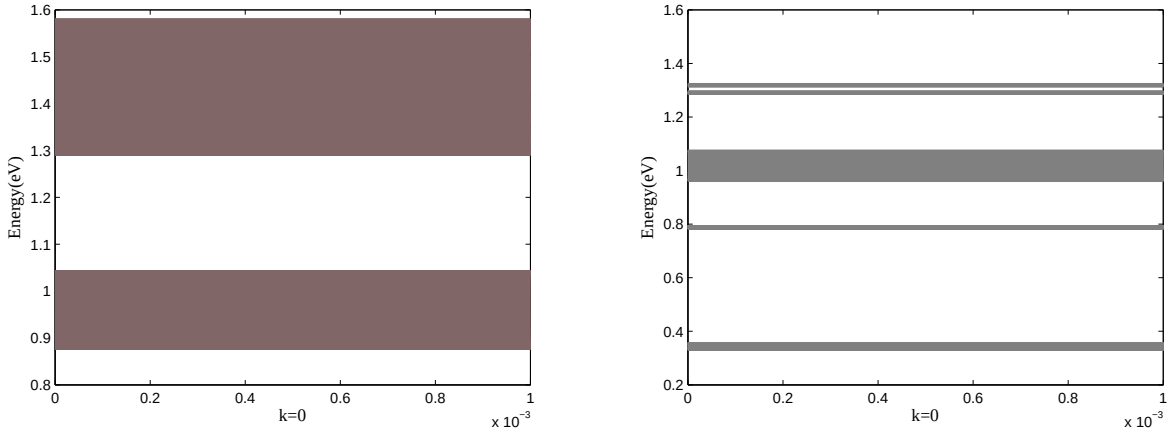

(a) (b)

Figure 3.33: Energy levels of system less than band gap (1.3 ev), for K=0 (a)200 truncated conical QD of size1, (b)200 truncated conical QD of size2)

Figures 3.31, 3.33, 3.27 and 3.29 demonstrate the result of simulation for 200 stacks of QD of different sizes and shapes. The result demonstrates that everything is similar to

result of simulation for 120 vertical stackes with same size QDs.

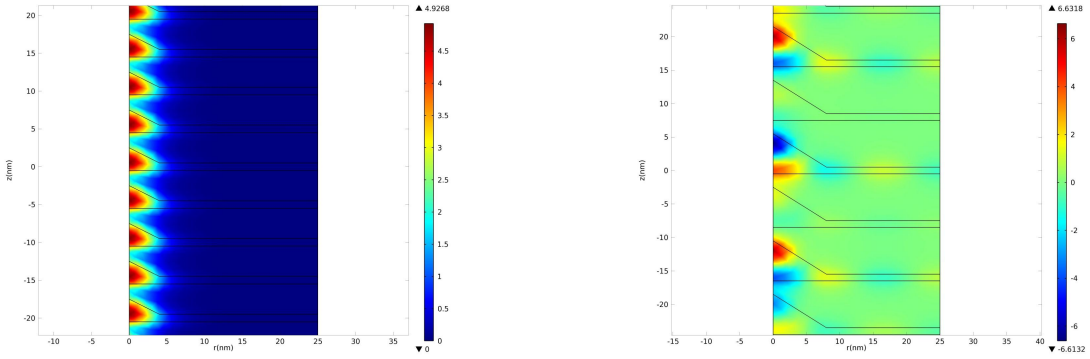

(a) (b)

Figure 3.34: Field distribution for (a) 200 conical QD of size1 plus wetting layer, energy level shown is 0.7029 ev (b)200 conical QD of size2 plus wetting layer, energy level shown is 0.0059 ev,(X axis: r(nm), Y axis: z(nm))

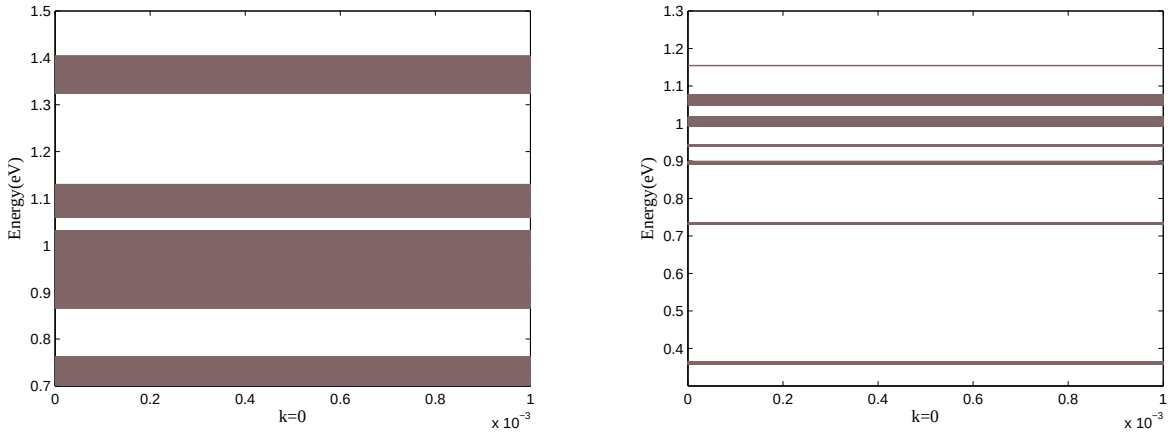

(a) (b)

Figure 3.35: Energy levels of system less than band gap (1.3 ev), for K=0 (a)200 conical QD of size1 plus wetting layer, (b)200 conical QD of size2 plus wetting layer)

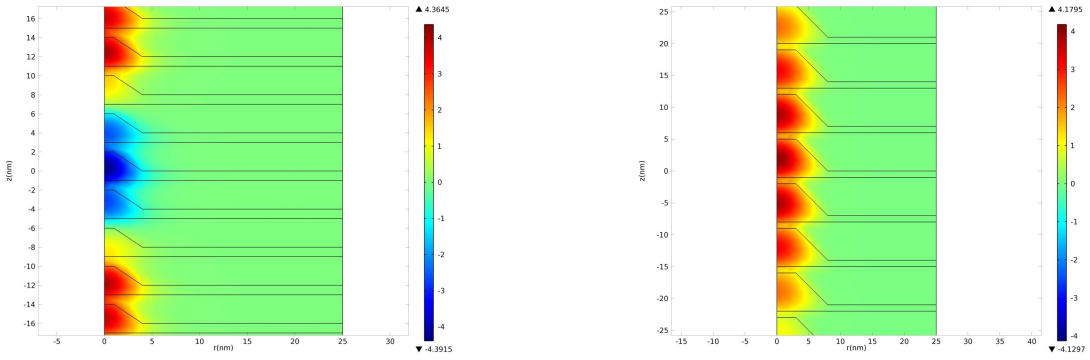

(a) (b)

Figure 3.36: Field distribution for (a) 200 truncated conical QD of size1 plus wetting layer, energy level shown is 0.6223 ev (b)200 truncated conical QD of size2 plus wetting layer, energy level shown is 0.2558 ev,(X axis: r(nm), Y axis: z(nm))

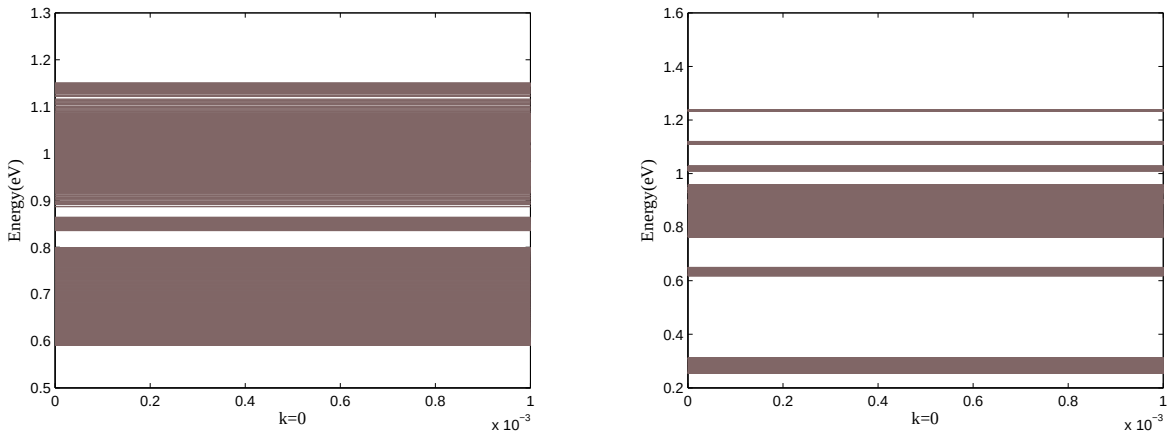

(a) (b)

Figure 3.37: Energy levels of system less than band gap (1.3 ev), for K=0 (a)200 truncated conical QD of size1 plus wetting layer, (b)200 truncated conical QD of size2 plus wetting layer)

When wetting layer is added minibands are formed as illustrated in figures 3.35 and 3.37 but, they are so close together that they are not able to provide the required energy bands for IBSC which is IB to CB band gap should be1.23 or 0.7 respectively. One possible solution to this problem is to find a material system that has very separated energy levels in a single QD. This may help to isolate the bands formed with presence of wetting layer further away from each other or to reduce wetting layer thickness as much as possible. Existence of wetting layer does not have significant effect on the energy levels of bigger size QD.

3.3 Matlab Simulation for QD Superlattices

Matlab has served as useful software for simulating QDs. It is a relatively easy software to work with. different approaches have been proposed for applying Matlab into the realm of QDs energy level research. Matlab has been utilized for finding energy levels of a single QD as well as finding energy levels of an array of QDs and has been so far the most popular software to find energy bands of IB cell.

3.3.1 Approaches for Simulation

There are two different approaches toward how to simulate one QD using Matlab. One is to simulate QDs using FDM method. The important thing is a suitable choice of grid size and shape. Then it requires solving huge matrixes of linear equations. The simplest case is cubic QD; in that case a square grid would be the choice and, this is the easiest type of grid to deal with. Other shapes would need more complicated grids and are harder to solve. This is an slow method which is suitable for one QD of different shapes [25, 46]. For an array of small number of QDs the time needed to solve linear equations is so big and, arithmetics are so slow that it would be impossible to simulate more than quite a few QDs using this method.

There are other approaches which could be used to simulate QDs or arrays of QDs using Matlab. These methods mostly rely on simplifying the QD structure or approximating Schrodinger equation. Some of these methods are plain wave expansion[25] approximating finite barrier with infinite barrier[47] and, Kronig- Penney model. Plain wave approximation requires very huge multidimensional matrices which are not easy to solve with

Matlab. Time and matrixes capacity dramatically increases with the increase of QDs in an array making it quite perplexing to solve. Approximating finite barrier would give a rough result since the barrier effect is eliminated. Kronig-Penney model is a relatively simple model for approximation of energy bands for a set of cubic QDs. Disadvantage of this approach is that, the actual shape of QDs should be approximated by a cubic QD of same size. For IBSC application another disadvantage is not including wetting layer. Nonetheless, its simplicity makes it a good choice for a primary estimation of energy levels.

Two sets of simulations have been carried out for this part, both along $< 100 >$ direction, one is a finite number of cubic quantum dots and the other one is infinite superlattice of cubic quantum dot. The first part is done by constructing propagation matric to find the transmission probability of QDs arrays. When the transmission probability, T, is 1 or similarly lnT is 0, there is a resonance through all of QDs; hence, a band is formed. With the same principals, Kronig -Penney model is applied to the infinite set of cubic quantum dots. Propagation matric is in the form of:

$$p = \frac{1}{2k_1k_2}\begin{bmatrix}(k_1+k_2)e^{-ik_2L} & (k_1-k_2)e^{ik_2L}\\ (k_1-k_2)e^{-ik_2L} & (k_1+k_2)e^{ik_2L}\end{bmatrix}\begin{bmatrix}k_1+k_2 & k_1-k_2\\ k_1-k_2 & k_1+k_2\end{bmatrix} \tag{3.11}$$

And the transmission probability derived from propagation matric would be:

$$Trans = \left[1 + \left(\frac{k_1^2 - k_2^2}{2k_1k_2}\right)^2 \sin^2(k_2L)\right]^{-1} \tag{3.12}$$

Kronig-penney model is of the form of:

$$\cos(ka) = \cos(\beta b)\cos[\alpha(a-b)] - \frac{\alpha^2+\beta^2}{2\alpha\beta}\sin(\beta b)\sin[\alpha(a-b)] \tag{3.13}$$

3.3.2 MATLAB Simulations for Different Structures

Matlab simulation has been done for three sets of structures. Conical and truncated conical QDs are approximated with a cuboid with same sizes of that of QDs. So, one has a8×8 rectangle and height 2 (size 1) and the other one 16×16 and height 5 (size2). Next is 60 arrays of cubiod QDs again for the two sizes. The last part is simulation of an infinite set of cuboid QDs. At the end, there is step by step comparison between Matlab Comsol simulations.

The first part is simulation of two QDs of size 2 and 1. Fig 3.38a shows that lowest energy configuration of conical QD of size2 is higher than energy levels of cuboid QD by 0.1 eV. But, energy levels of cuboid QD match with energy levels of the truncate QD of size2. shows cuboid QD of Matlab simulation has lower energy levels than conical quantum of size1 by 0.2 ev and truncated QD by 0.1 ev.

Both of these Matlab simulations will not be accurate when wetting layer is added as Comsol Figures demonstrated.

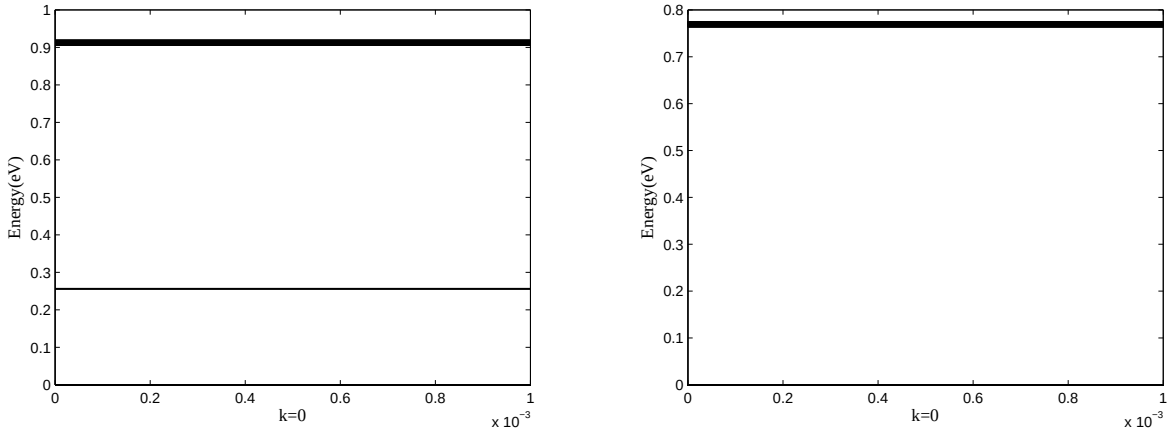

(a) (b)

Figure 3.38: Energy levels of system less than band gap (1.3 ev), for K=0 (a)1 cuboid QD of size2, (b)1 cuboid QD of size1

Next step is simulating 60 QDs of cubic shape with two sizes 1 and 2 using propagation matrix.

Looking at the result of Matlab simulation in Fig. 3.39a for 60 QDs of cubic shape with size 2 and, comparing it with Comsol simulation of same numbers of conical and truncated conical QDs it is revealed that propagation matrix of cubic QDs simulation produces lower energy levels than Comsol conical QDs by 0.2 ev, however, has almost same energy levels compared to truncated QDs of Comsol simulation. Band width of Matlab simulation is wider apposed to Comsol simulation that has almost no band width for energy level starting from 0.8 ev. Comparing Fig. 3.39b with result of 60 QDs of conical and truncated QDs of Comsol it would be understood that Matlab simulation energy levels are lower

than energy levels of Comsol simulation by 0.3 ev and 0.2 ev for conical and truncated QDs respectively.These two simulations again are not valid when wetting layer is added due to substantial effect of wetting layer on energy levels as could be seen in Comsol simulation.

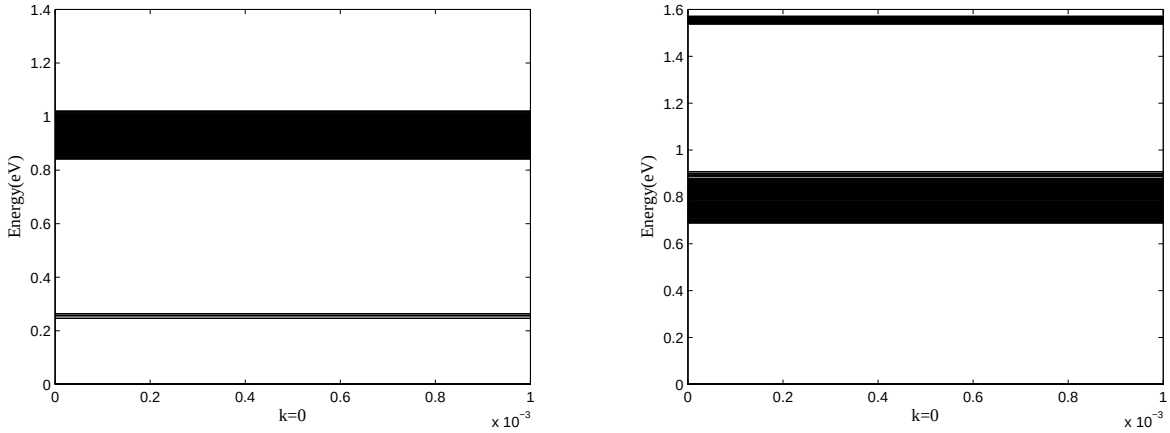

(a) (b)

Figure 3.39: Energy levels of system less than band gap (1.3 ev), for K=0 (a)60 cuboid QD of size2, (b)60 cuboid QD of size1

The simplest method used to find band structure of an infinite array of periodic potential is using Kronig-Penney model. In this part this method has been employed to find the band structure of infinite array of cubic QDs with two sizes 1 and 2 and, then compare it to the results of Comsol for 200 numbers of conical and truncated conical QDs.

Kronig-Penney simulation for infinite array of cubic QDs of size 1, Fig. 3.40a has an energy band from 0.5 to 0.62 which is 0.5 ev lower than array of 200 conical QDs and, 0.4 ev lower than 200 truncated conical Qds. But, next energy band of this simulation is around 4 ev which is far away from 1.3 ev which is the second energy band of both conical and truncated QDs. The same simulation for an infinite array of cubic QDs has been carried out, this time for size number 2, Fig. 3.40b. Again energy bands overall are less than conical and truncated conical QDs. The reduction is around 0.2 ev. This shows that for lowest energy configuration infinite array of cubic QDs could give somewhat a reliable approximation of truncated conical QDs. Albeit, adding wetting layer to system would change the whole system; thus, this Matlab simulation could not a simple estimation of

energy bands.

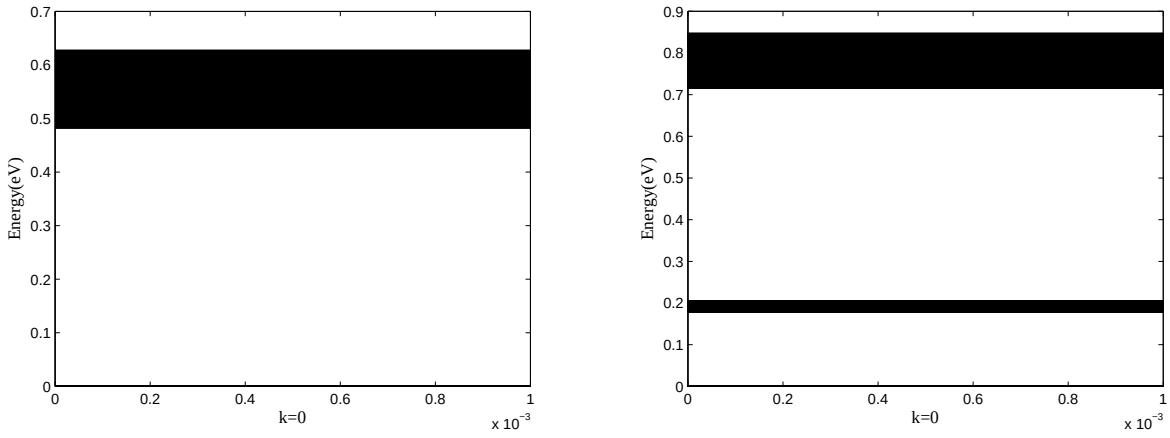

(a) (b)

Figure 3.40: Energy levels of system less than band gap (1.3 ev), for K=0 (a)infinite cuboid QD of size, (b)infinite cuboid QD of size1

Matlab simulation and the Comsol counterpart comparison shows that, all Matlab simulations are not valid at the presence of wetting layer; therefore, it is not possible to use Matlab for band energy finding if MBE is used. Secondly, truncated QDs have a better match in both simulations. This is due to the fact that its shape is closer to cuboid. To use Matlab as the main simulation method the shape of QD should not be far from cuboid. if precise knowledge of bands are required Comsol would be a better option. Matlab results corresponds to l=0 result of Comsol. If l is greater than that matlab and Comsol result do not match at all.

Chapter 4

Colloidal QDs Supper Lattice: A Potential Approach to Intermediate Band Solar Cell

Molecular Beam Epitaxy (MBE) is the most applied method for fabrication of quantum dot arrays embedded in a lattice matched layer to work as active layer of Intermediate Band Solar Cell (IBSC). Using this method for this purpose however is expensive and complicated. Therefore, exploring alternative simple and low cost approaches for growing quantum dots (QDs) self-assmbled layers is of great interest. Finding such an alternative method is not trivial due to unique properties of super lattice structures which match the criteria essential to obtain IB effect. Recent research results indicate the great potential of colloidal QDs to use as the active layers of new generation of QD based solar cells. Moreover, the material synthesis is low cost and easy to deploy. Two and three dimensional QD superlattice structures can be obtained by colloidal QD self -assembly which can be utilized in IBSC devices. Obtaining large numbers of stacked self-assembled layers is possible with use colloidal QDs, something has been proven hard to be feasible using MBE method

Materials which are used for MBE self-assembly are III-V group which have very low effective mass. Low effective mass helps for better separation of bands in QDs, so will reduce fast carrier relaxation rate which makes band formation possible. However, materials for colloidal QD synthesis are chosen from group II-VI, these QDs have higher effective mass compared to III-V, and their conductivity is lower due to the presence of dielectric ligands, poor exchange coupling and presence of dangling bounds. This process also allows

the chemical functionality of the organic capping layer to be precisely adjusted. Research is ongoing in this field in order to overcome these barriers to let this technique to compete with other sorts of QDs layer and, superlattice fabrication methods. For instance, a possible solution for improving electron transportation and conductivity of colloidal crystals could be ligand exchange. Common organic ligands used in QD synthesis are relatively long and dielectric. Changing these ligands with short organic ligands or metallic ones could improve conductivity substantially. Another possible approach is crosslinking of QDs with organic molecules and then adding electrons to the system via electrochemistry Despite the existing unsolved problems, colloidal QDs superlattice fabrication is become a growing and an attractive research area due to its fast, cheap and defect free characteristics.

Methods such as Langmuir-Blodget (LB), self-assembled monolayer (SAM), Layer by layer (LBL), Electrophoretic deposition (EPD) and evaporation driven self-assembly (EDSA) are dominantly reported in literatures for fabrication of QD self-assembled layers. The dipcoating has not been yet reported as a comprehensively developed method. Dipcoating is precisely controlled immersion and withdrawal of any substrate into a liquid vessel in order to deposit a layer of material. This method is simple, repeatable and cost effective and the key factors contribute to determining the state of the resulted dip coated thin film could be precisely controlled. A large variety of repeatable dipcoated film structures and thicknesses can be fabricated by controlling the functionalisation of the initial substrate surface, submersion time, withdrawal speed, number of dipping cycles, solution composition, concentration, viscosity, temperature, number of solutions in each dipping sequence and environment humidity. The dip coating technique is used for the fabrication of thin films with thicknesses of exactly one monolayer or it can create films of increased, precisely controlled thickness.

In this chapter growth of closed packed monolayer and multilayer self-assembled colloidal QDs is investigated using dipcoationg method. We examined the effects of QD concentration, QD size, submersion time, withdrawal speed, surface area, boiling point and polarity of the solvent and substrate surface state on the structure of the layer. Photoluminescence (PL) fluorescence imaging , AFM (Atomic Force Microscopy), High Resolution Secondary Electron Microscopy (HRSEM), TEM (Transmission Electron Microscopy), High Resolution Transmission Electron Microscopy (HRTEM), Electron Energy Loss Spectroscopy (EELS), Energy-dispersive x-ray Spectroscopy (EDS) and Scanning Transmission Electron Microscopy (STEM) were performed to analyze the obtained layers. In the following sections we present the results of our experiments.

4.1 Experimental Setup

Experiments have been done using KSV NIMA dipcoater which is shown in Fig. 4.1a. Software-controlled deposition features include setting the upper and lower substrate resting positions, immersion speed, submersion period, withdrawal speed, drying period, and number of dip cycles. The different components of the system are shown in Fig. 4.1b. the dipping arm is connected to the sample holder and its upward and downward movement is controlled by a DC motor that provides smooth linear motion of the substrate at all dipping speeds. In order to have a better control on the drying rate of the solvent which was found an important factor in the film structure, we designed, fabricated and added a shield to the system.

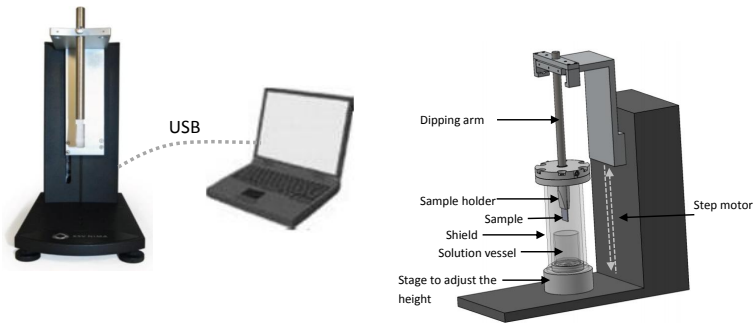

(a) (b)

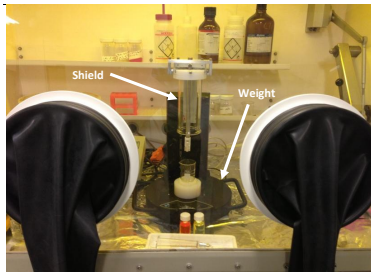

(c)

Figure 4.1: a) KSV NIMA dip coater, b) diagram describing different part of the dipcoater, c) glovebox under nitrogen working place of the experiments.

Experiments started to be carried out with the system shown in Fig.4.1a. at the beginning, but there existed disturbance in the form of vibration in our set up. As mentioned

earlier, other problem arose from the fact that solution was evaporating. Since any changes in the whole solution during dipping process was not desired, this inevitable phenomenal was another source of imperfect condition. To remove all these nonidealities we added a shield to reduce evaporation, a weight to reduce vibration and, we moved dipcoater in the glove box under nitrogen to eliminate oxygen, moisture and dusts that offers reproducibility of samples. Moreover, glove box is a safe place while working with toxic QDs materials and chemicals. The final setup used for the experiments is shown in Fig.4.1a.

4.2 Schematic Illustrations of the Dipcoating Process

In a dip-coating process, a substrate is dipped into and withdrawn from a liquid coating solution at a controlled speed. Faster withdrawal speed results in increase in the layer thickness. The thickness is determined by the balance of forces at the stagnation point, a point in a flow field where the local velocity of the fluid is zero, on the liquid surface. More fluid pulls up onto the surface of the substrate at a faster withdrawal speed before it has time to flow back down into the solution. Fluid viscosity, fluid density, and surface tension are the main parameters that affect the thickness of the layer(see Fig.4.2).

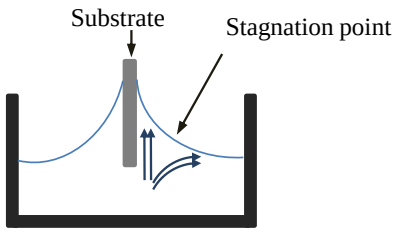

Figure 4.2: Schematic diagram of the dipcoating process

Dip-coating is an excellent method for formation of high-quality and uniform layers; however it requires precise control and a clean environment. The coating remains wet for several minutes until the solvent evaporates. A variety of methods including conventional thermal, UV, or IR techniques can be used to cure the layer depending on the coating solution formulation in order to accelerate the drying process. A multi-layer stack can be

constructed by applying other layers on the first one with consecutive dip-coating/curing processes.
Colloidal crystals are QDs with narrow size distributions deposited from solvents and assembled into nanocrystal superlattices. Depending on the solvent polarity, the interaction between QDs becomes slightly attractive by solvent evaporation which leads to formation of concentrated dispersion. The boiling point of the solvent needs to be in the range to permit the QDs enough time to find equilibrium lattice sites before the solvent evaporates on the growing structure. The weak vander Waals and dipolar magnetic attractions hold the nanocrystal superlattices as solids. Organic groups that cross link upon exposure to radiation or heating can be used to make these structures more rigid [48].

4.3 Experiments

20mg of CdSe/ZnS colloidal QDs stabilized in octadecylamine (ODA) with narrow size distributions dispersed in 5mL toluene and chloroform was purchased from the manufacturer (NN-Labs Inc.). Experiments were performed on three different sizes QDs; Yellow (diameter 5.5), orange (diameter 6nm) and red (diameter 6.5nm) with absorption peak at 520nm, 591nm and 620 nm respectively. The self-assembly process was examined on quartz and silicon substrates. At the first stage the main concern was observing self-assembly of QDs not the applicability of substrate for IBSC device. Silicon itself may not be the best choice for IBSC device due its small band gap and low carrier mobility; however, once the optimum condition is found on silicon, transferring the process to another substrate would require fine adjustment and take much less time. Piranha and RCA1 were used to improve the wettability of the initial substrate surface. As a result solution remains on the surface for longer time which permits the QDs more time to find equilibrium lattice sites before the solvent evaporates on the growing crystal. In addition to QD size, substrate type and their surface treatment, withdrawal speed, sample area, submersion time, solution composition: QD concentrations per volume and number of dipping cycles were also tuned to obtain self-assembled structures.

Sample 1

The first sets of experiments were performed on RCA1 cleaned quartz and $< 100 >$ silicon substrates with $1cm \times 2cm$ ($immersionheight \times width$) sample area at withdrawal speed of 5 mm/min, with no submersion time. The solution was prepared by injecting

0.3mL of stock solution red QDs into 20mL of toluene. Fluorescence imaging were conducted on the selected sample 1 of this set with quartz substrate using Photoluminescence (PL) system from Edinburgh Inc. equipped with microscope, 20X objective and beam spot size of 400m2. PL fluorescence image in Fig 4.3a shows that there is non-uniform coverage of QDs over the surface. QDs do not follow any pattern and are randomly distributed over the substrate and, they are agglomerated together in some spots. PL measurements for silicon samples for this set were completely dark showing either QDs are not optically active or with these conditions no QD coverage on the surface of silicon occurred.

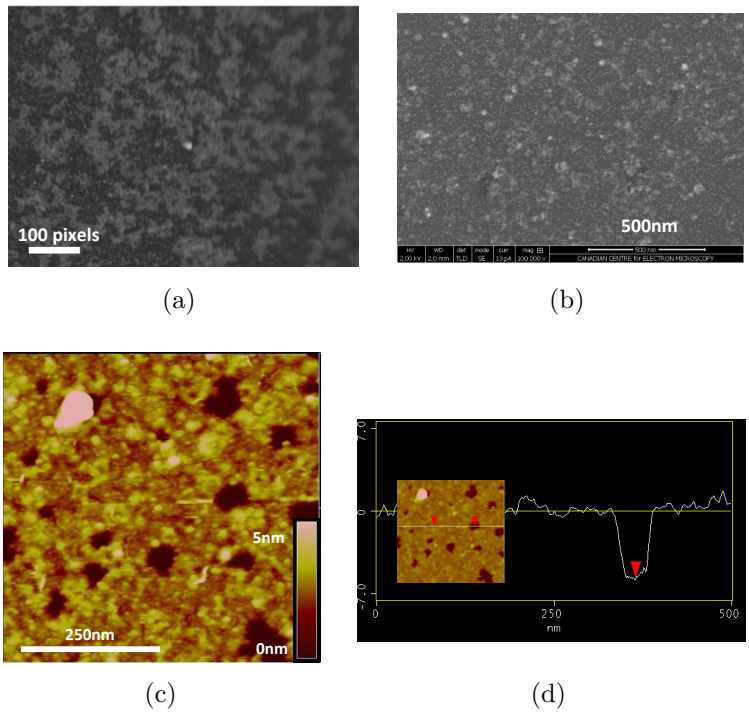

Figure 4.3: Morphology of the dipcoated layer on sample 1: prepared on RCA1 cleaned 1cmX2cm quartz substrates, at withdrawal speed of 5 mm/min, no submersion time, dipped in a solution containing 0.3mL stock solution red QDs injected into 20mL of toluene: a) Flouresence, b) HRSEM, and c) AFM height images. d) AFM profile data correspond to the white line (see inset).

PL fluorescence image gives a rough idea about the QD layer. Due to the small size of the QDs this method is not capable of showing details of the morphology of the layer. For

obtaining more comprehensive ideas AFM, HRSEM and TEM, EELS, EDS and STEM were conducted for upcoming selected samples.

Fig. 4.3b shows HRSEM image of this sample. It seems that for this type of samples the information that can be provided by HRSEM is close to the fluorescence image of the sample meaning that the resolution of this method is not high enough to see the QD layer structure more clearly. It was concluded that to study the QD layer structure AFM and TEM should be consider as primary methods. Fig. 4.3c indicates the AFM height image of the sample 1 taken in tapping mode. AFM shows a clearer picture of the top most deposited layer. The image shows a partial QD coverage on the surface beside presence of agglomerated sites. Fig.4.3d illustrates the AFM profile data correspond to the white line: the height measurement between arrows is 6.5nm which corresponds to manufacturers data for red QDs, also indication that the despite the layer partially covered the surface, it is monolayer.

For meticulous investigation of numbers of QDs layer and, for a closer look of arrangement of QDs TEM, HRTEM and in-situ EDS analyses were conducted. Focused ion beam (FIB) milling techniques used for TEM specimen preparation. Fig. 4.4a shows the final sample prepared by FIB. There is no way to choose the desired part of the sample using this technique. It selects a very small random part of sample. In order to protect the layer from the ion milling, prior the FIB process, QDs were embedded in silicon nitride layer of about 90nm deposited by plasma Enhanced Chemical Vapor deposition (PECVD) at silane to ammonia gas ratio of 0.5 with the flow rate of 20:40 silane: ammonia, plasma pressure of 0.6 Torr and plasma power of 23w at 175C. TEM image of sample 1 show ordered monolayer of QDs capped with SiNx layer (see Fig. 4.4c). In the part that happened to be selected for FIB there was no void and one layer of QDs could be seen in this image. These images show the possibility of embedding QDs in another material without damaging them. The HRTEM in Fig. 4.4b indicates the shape, size and crystal orientation of the QDs.

Electron Energy Loss Spectroscopy is an appropriate method to accurately analyze the thin layers. We performed EELS on sample 1. Fig.4.5a and Fig. 4.5b show the dark field image of the sample and the maps provide for Zn, Si, O, Cd, N and C within the region selected in green box respectively. The sum spectrum of the elements was extracted from the EELS data (see Fig. 4.5c). The spectrum shows that the N and Cd peaks are overlapping, since there is much more N present, the map mostly represent N. The S and Se signal is not strong enough to create a map. Zn is also very weak which is expectable

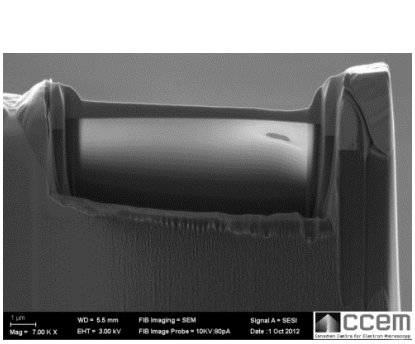

(a)

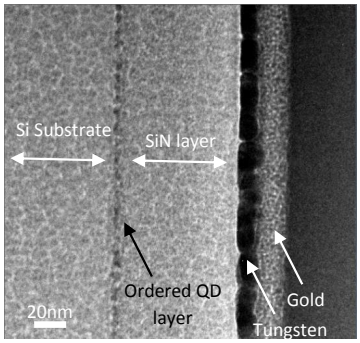

(b)

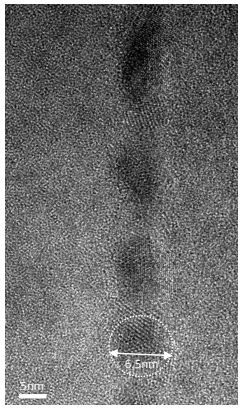

(c)

Figure 4.4: a) Sample prepared by FIB, b) ordered monolayer of QDs capped with SiNx layer, c) HRTEM image of (b).

due to the composition of QDs which mainly contains of Cd. The percentage of Se, Zn and S is very low. QDs are passivated with a very thin layer of ZnS (1nm). Detection of carbon is due to the presence of organic ligands attached to the QDs outermost surface.

Sample 2

In order to decrease the voids in the QD layer, speed of immersion was slowed. It is believed that speed plays the most important role on the QDs tendency to attach to the surface since slower movement of sample inside the solution introduce fewer disturbances to QDs arrangement. As a result, QDs have more time to find equilibrium lattice sites and

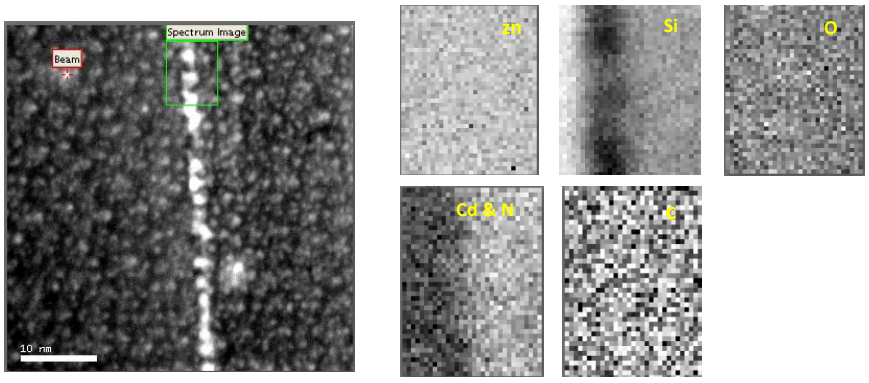

(a) (b)

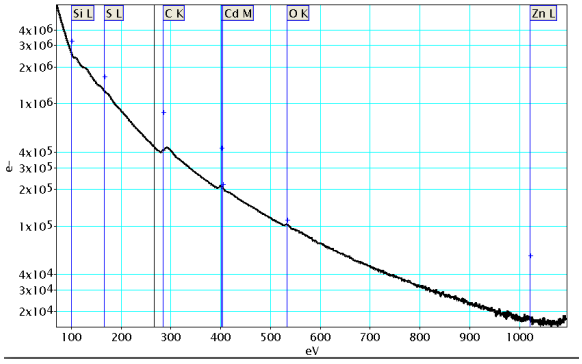

(c)

Figure 4.5: a) Dark field image of the layer(scale bar: 10 nm), b) map image of different elements in the green box shown in (a), c) extracted spectrum with the peaks corresponding to the elements present in the layer

their movement will not be disturbed as well. Concentration of the QDs in the solution is another factor that plays a major role in self-assembly process since increasing number of QDs in solution would bring more possibilities of QDs to contact with the substrate surface. In the next experiment these two parameters were altered.

In this experiment withdrawal speed was reduced to 0.5 mm/min and solution was prepared by injecting 0.9mL of red QDs stock solution into 20mL of toluene. The rest of parameters were remained unchanged. Fig.4.6 indicates the fluorescence images of this

sample, taking from different parts of the sample. Ordered lines of glowing QD particles can be seen in the PL images which is an indication of having ordered layer formed on the surface. Since sample could not be judged from PL image only, AFM was performed for further investigation.

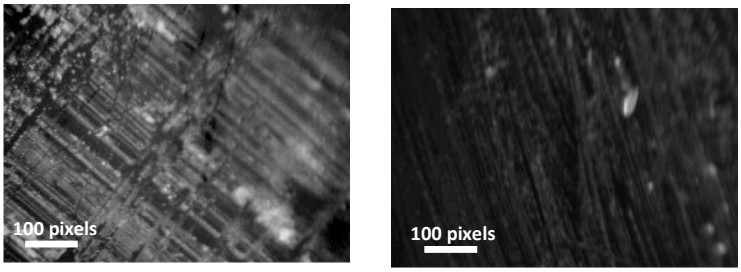

(a) (b)

Figure 4.6: PL fluorescence images of different parts of the sample 2

AFM images shown in Fig.4.7a demonstrate partial monolayer coverage of hexagonally closed packed (hcp) QDs formed on the substrate. But this time there is no agglomeration sites of QDs can be observed. Fig.4.7b-top shows the AFM profile data correspond to the white line: the height measurement between arrows and also for the entire line is 0nm which another indication of formation of uniform monolayer of QDs. In AFM profile data shown in Fig. 4.7b-bottom the height measurement between arrows is 7nm which is close to the size of red QDs.

Sample 3

In this experiment we kept all the conditions similar to sample 2 except the immersion height in order to see the effect of decreasing surface area of sample entering the solution on surface coverage. Sample height was reduced to 7 mm, resulting in $7mm \times 2cm$ surface area of sample entering the solution. Fig. 4.8a and Fig4.8b show the height (top) and corresponding phase (bottom) AFM image of sample 3 in 1m and 250nm scale respectively. Fig. 4.8c indicates the AFM profile data of the image shown in Fig. . The height measurement for the line on the part of image with uniform layer is 0 (top image) and on the line crossing the voids is equal to QD size (bottom image) which is an indication of formation of uniform monolayer of QDs on this sample. Not much difference was observed

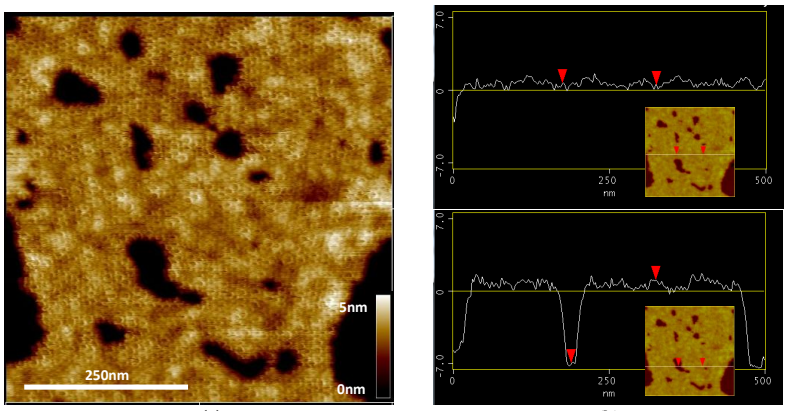

(a) (b)

Figure 4.7: a) AFM height image of sample 2: withdrawal speed of 0.5 mm/min and solution containing 0.9mL of red QDs stock solution in 20mL of toluene, showing hcp crystal structure of QD layer, b) AFM profile data correspond to the white line (see insets) for different part of the layer.

between sample 2 and sample 3. Again the condition seemed to work for quartz only; there was not noticeable improvement on silicon samples.

Sample 4 and sample 5

We also investigate the effect of solvent with higher evaporation rate on the structure of the layer. Instead of toluene this time chloroform was introduced to the solution. Since the withdrawal speed was relatively slow, experiments took long time (5hours). Fast evaporation rate of chloroform damaged the tranquil surface conditions. In order to overcome this problem, we can either mix the chloroform with toluene to tune the solvent evaporation rate or add a shield to the set up as explained earlier.

Sample 4 and sample 5 were prepared using chloroform as the solvent and Piranha to promote the wettability of the surface. The rest of parameters remained same as sample 3. The AFM images in Fig.4.9a and Fig.4.9b show the structure of the layer formed on silicon (sample 4) and quartz (sample 5) substrates respectively. Comparing these two images we conclude that Piranha has improved wettability of silicon substrate as oppose to quartz. The second layer is start forming on the silicon substrate (see the AFM in Fig.4.9a and

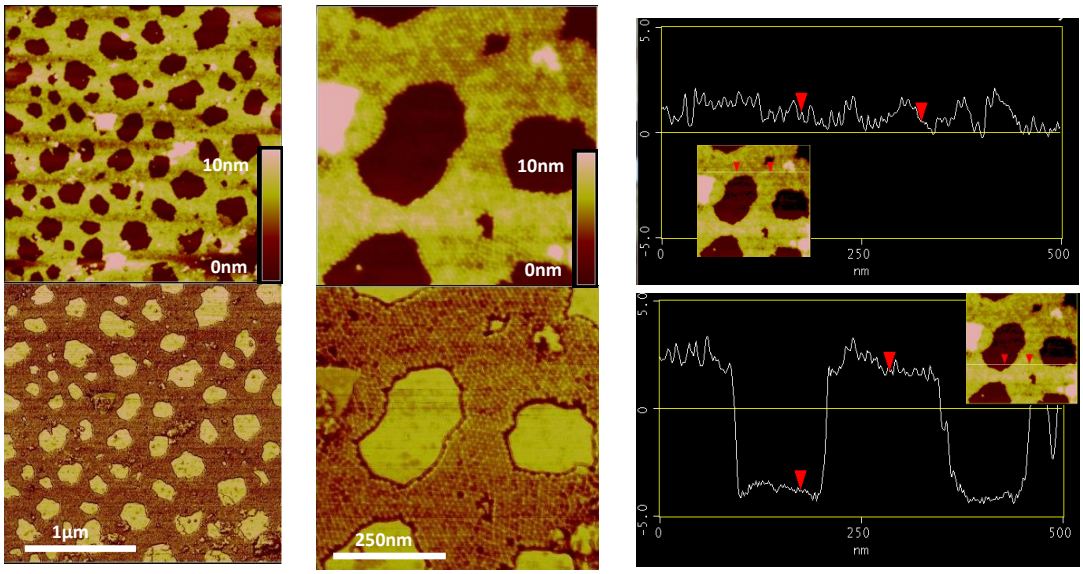

(a) (b) (c)

Figure 4.8: Height (top) and corresponding phase (bottom) AFM image of sample 3: surface area of $7mm \times 2cm$ a) scale bar=1m, b) scale bar=250nm, c) AFM profile data correspond to the white line for different part of the layer.

profile data in Fig.). However, considering the fact that applying Piranha is very dangerous since it can explode fairly easily, the rest of experiments were carried out using RCA only.

Sample 6

From the results of sample 5 we observed that Piranha helps for better coverage for silicon substrate than quartz. On the quartz there are many uncovered spots while it seems that for the silicon there is complete coverage but random distribution and, there is more than one layer. To see whether increasing number of dipping cycles would improve coverage on quartz substrate sample 6 prepared with the same conditions as sample 5 but dipped 16 consecutive times. AFM result in Fig.4.10 illustrates that coverage is more but not complete and, there are huge columns of agglomerated QDs layers.

QDs arrangement on all Piranha prepared samples seemed to be randomly piled up

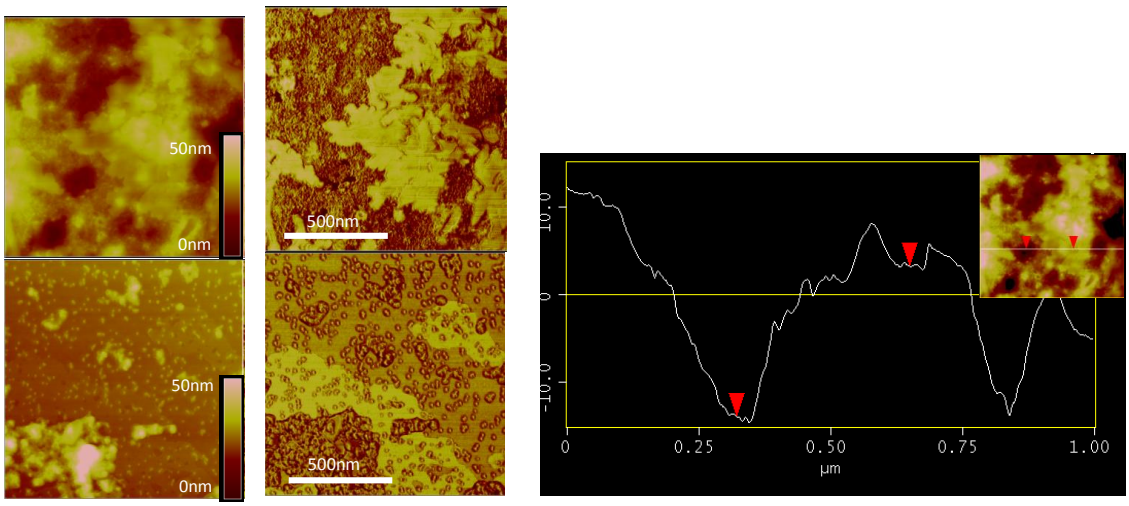

(a) (b) (c)

Figure 4.9: height (left) and corresponding phase (right) AFM image of samples prepared using chloroform as the solvent and Piranha to promote the wet-ability of the surface on a) silicon (sample 4) and b) quartz substrates (sample 5), c) AFM profile data of (a) correspond to the white line (see inset).

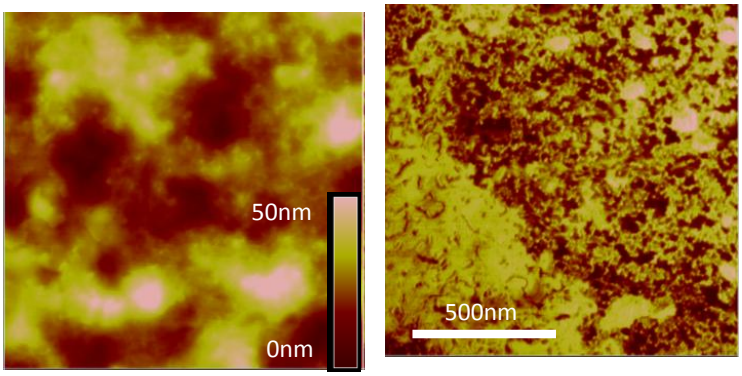

(a) (b)

Figure 4.10: Height (left) and corresponding phase (right) AFM images of sample 6: 16 times dipping cycles of Piranha treated quartz substrate.

and, AFM was not able to give comprehensive information about the layer. TEM and HRTEM images shown in Fig. 4.11 demonstrate that QDs are piled up without following any closed-pack pattern. Sites with higher contrasts in HRTEM image are crystalline QDs surrounded by tiny amorphous layer of organic ligands that can be seen as sites with lower contrasts.

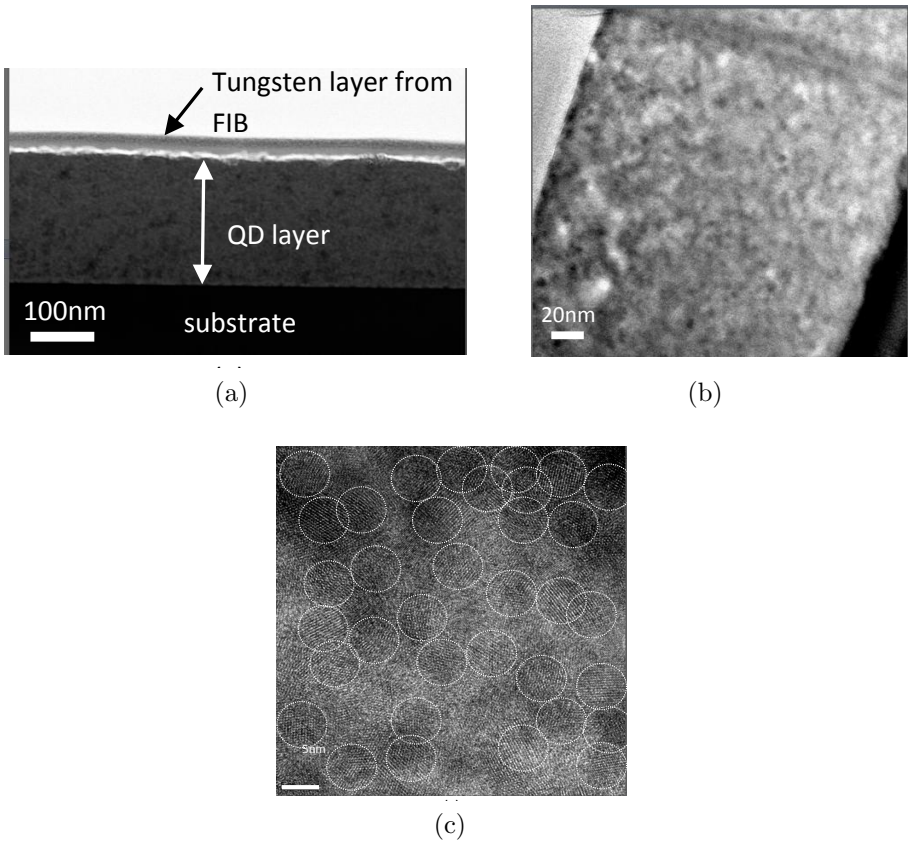

(a) (b)

(c)

Figure 4.11: a) high and b) low magnification TEM image of sample 6: 16 times dipping cycles of Piranha treated substrate , c) HRTEM image of (a)(circles are 5nm).

Since the layer is thick, we performed EDS to study the existence of different elements in the layer. Fig.4.12b is the spectrum corresponding to the area in the QD layer which is under electron beam exposure as indicated with red cross in Fig.4.12a. STEM results in Fig.4.12c present the spectrum of each element along the yellow line in the top-left image. The results indicates that the dominant elements in the layer are Cd, Se, Zn and S. The

presence of the carbon is again because of the coverage of QDs with organic ligands. Nitrogen and oxygen can be attributed to the chemical reaction of QD layer with the ambient.

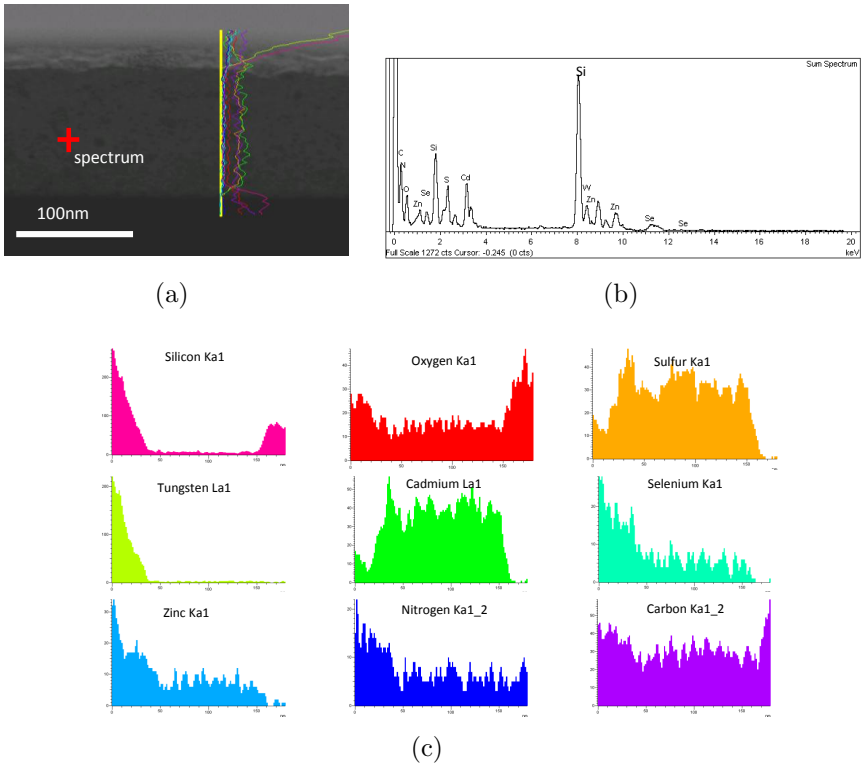

Figure 4.12: . a) Area in the QD layer which is under electron beam exposure for both b) EDS and c) STEM analyses indicating sum and distinct spectrum of components present in the QD layer respectively.

Sample 7

Next set of experiments were carried out by increasing concentration of QDs from previously 0.9 mL in 20 mL of toluene to 1.2 mL. Also, withdrawal speed was decreased from 0.5mm/min to 0.1 mm/ min and submersion time was added to the system. When sample was completely immersed in the solution there was a halt for 500 s. no movement allowed at that time and, immersion areas was reduced to $7mm \times 1cm$. Another turn point was that from this experiment we mainly worked on silicon substrates instead of quartz. Firstly, quartz is not a suitable material for IBSC fabrication Secondly, the difficulty of QDs at-

tachment on Silicon substrate was diminished. QDs under above condition showed good surface coverage on silicon substrate either. Height and corresponding phase AFM image of sample 7, are shown in Fig. 4.13. AFM result show partial coverage of QD layer on silicon substrate. Perhaps this can be due to the low concentration of QDs in the solution and short submersion time.

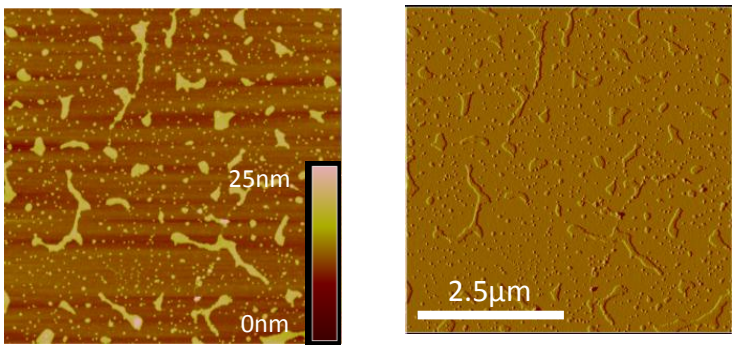

(a) (b)

Figure 4.13: Height (left) and corresponding phase (right) image of sample 7: 1.2 mL of QDs in 20 mL of toluene at withdrawal speed of 0.1 mm/ min and submersion time of 500s for a RCA1 treated $7mm \times 1cm$ silicon substrate.

Sample 8

To examine whether submersion time does have any effect on QDs layer formation next sample (sample 8) was prepared with exactly same condition except for the submersion time which this time increase to 3600s. Height and corresponding phase AFM image of sample 8 in Fig. 4.14a and Fig.4.14b show that there are areas of surface almost empty and other parts of surface are agglomerated and have built up very huge pyramids of QDs. It could be concluded that there should be an optimum for waiting time since this very long period had more destructive effect and caused huge pyramidal agglomeration of QDs to occur.

Sample 9

In the next experiments the smallest size yellow QDs was introduced in the solution.

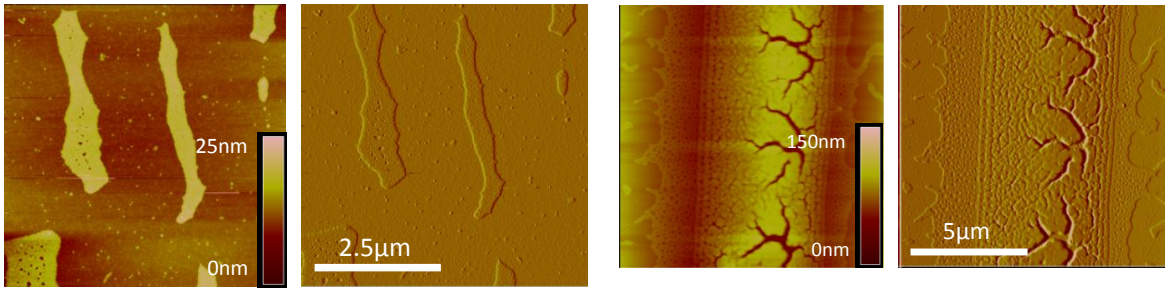

(a) (b)

Figure 4.14: Height (left) and corresponding phase (right) image of sample 8:submersion time of 3600 s, a) low percentage partial coverage of an area on surface, b) other part of surface with agglomeration of QDs that built up very huge pyramids of QDs.

The sample was prepared under condition same as sample 7: 1.2 mL of QDs in 20 mL of toluene, withdrawal speed of 0.1 mm/min and submersion time of 500s prepared on a RCA1 treated $7mm \times 1cm$ silicon substrate. Submersion time also increased to 600s. AFM images in Fig. 4.15a shows that smaller QDs help for much better coverage of surface in areas as large as 5m2. The profile data in Fig. 4.15b shows partial monolayer coverage of QDs on the substrate.

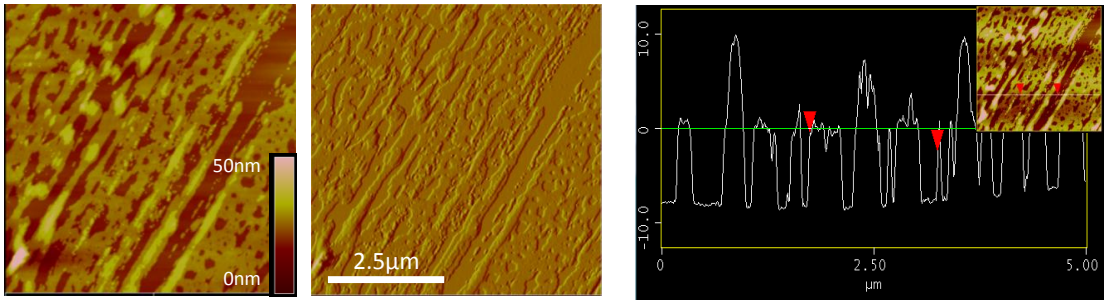

(a) (b)

Figure 4.15: Higher percentage of partial monolayer coverage on silicon substrate by using smallest size yellow QDs and submersion time of 600s; a) Height (left) and corresponding phase (right) image of sample 9: scale bar=2.5m, b) The profile data of (a) correspond to the white line (see inset).

Sample 10

Having seen the good coverage of sample 9 the next sample, sample 10, was prepared with the same condition except for the concentration. Solution was prepared by injection of 3mL of yellow QDs in 20 mL of toluene. The rest of conditions remained the same. AFM image demonstrate that although there is still tiny holes in 5m2 area of the sample (see Fig.4.16a) full monolayer coverage of self-assembled QDs for areas of 1 μm^2 (see Fig.4.16b) and 500 nm^2 (see Fig. 4.16c) is obtained. This condition can be reported as the best condition for the self-assembled monolayer formation so far.

From the height AFM image we can tell that the second layer is forming on the first layer. The phase image shown in Fig.4.16c shows that the same pattern on the top layer and the bottom layer depicting the partial monolayer coverage of the second layer on the previously formed first layer. The profile data shown in Fig.4.16dtop depict the high percentage of monolayer coverage on the surface with small voids. Fig. 4.16dmiddle and Fig.4.16dbottom show high surface roughness which is due to the formation of the second layer.

Sample 11

To investigate whether lowering the withdrawal speed would offer more benefits for QD arrangment and attachment to the surface or not, sample 11 was prepared with the same condition but with lower speed. Speed decreased to 0.05 mm/min. AFM result reveals that there is an optimum value for speed. Increasing or decreasing speed more than this point would dergrade the optimum condition. As it could be seen in AFM images, lowering the withdrawal speed results in larger holes. The AFM images shown in Fig. 4.17a and Fig.4.17b are provided from different area of the sample. These images and their corresponding profile data (see Fig. 4.17c and Fig.4.17d) indicate that the percentage of partial monolayer coverage is differ from one location to another location of this sample.

The TEM analysis was performed for sample 11 (see Fig.4.18a). The TEM image shows that there are two layers of quantum dot on top of each other. HRTEM image implies that double layer structure is close to closed-pack self-assembly (see Fig.4.18b). Fig.4.18c illustrates the top and cross section view schematic structure of two consecutive hexagonally closed packed (hcp) QD layer. The structure observed in Fig.4.18b is close to this structure. One reason for deviation from a perfect hcp structure could be the lack of size and

shape monodispersity. Even a small asymmetry in shape and size would disturb perfect hcp QD layer formation. Sample 11 also shows the possibility of self-assembly of more than one layer by single dip.

Experiments after Addition of Shield to the Setup

From this part the shield shown in Fig. 4.1b,4.1c was added to the dipcoater setup. The main role of this part is to reduce the presence of contamination close to experiment area as well as reducing evaporating rate of solution especially if highly volatile solutions, for instance, chloroform, are being used.

Three other major changes were made in these sets of experiments. Firstly, silicon SiNx and zinc oxide (ZnO) layers were also introduced. ZnO could serve as a possible candidate for IBSC device since it has a large band gap. When QDs are embedded in ZnO, the 3-D quantum confinement will occur. SiNx is a good candidate to improve the wettability of the surface. Next important change was using one solution in more than one experiment. Previously a new solution was prepared for each experiment but, for this part one solution was used more than once. This can potentially reduce the cost of the process by reusing the materials without requiring changing them for the experiments conducting under approximately same concentration.

sample 12 and sample 13

Sample 12 was prepared with injection of 2 mL of orange QDs from the stock solution in 10 mL toluene. Solution was reduced from 20 mL in previous experiment to 10 ML in this new one. The experiment performed on sputtered ZnO layer at the withdrawal speed of 0.05 mm/min, submersion time of 600s. Sample 13 was prepared by using the same solution but on Si substrate and, this sample was dipped 3 times. AFM images in Fig. 4.19a, 4.19b and Fig. 4.19c,4.19d show the surface morphology for sample 12 and 13 respectively.

Images show that QDs have covered the surface of ZnO substrate in clusters and, they do not follow any pattern. One possible reason for that could be due the morphology of the starting sputtered ZnO layer. It does not have crystalline orientation which causes the QDs to form as clusters. The 3D height AFM image indicates the high roughness of the QD layer formed on ZnO layer. AFM results in Fig.4.19c,4.19d show that even after 3 times dipping

still there are voids on the silicon substrate. One reason could be effect of adding shield to the system. This shield would change the environment providing that this condition is not exactly the same as sample 10 that resulted in complete coverage in $1\mu m^2$ surface area.

sample 14 and sample 15

Next set of experiments were carried on PECVE deposited silicon nitride layer (sample 14), and silicon substrate (sample 15). The latter was dipped 3 times. The only difference of these samples with sample 12 and sample 13 is the use of yellow QDs which has smaller size. This was done to check which size of QDs is more suitable for self-assembly. Again the solution was the same for both samples. AFM results for sample 14 and sample 15 are shown in Fig.4.20a and Fig. 4.20b respectively.

These images show that QD coverage on Si surface after 3 times dipping is still lower than SiNx surface. Silicon nitride seems to offer a good surface wettability.

sample 16

Sample 15 is still far from the perfect coverage of sample 10. To check whether this deviation is a result of deviating from the ideal condition of sample 10 or because of addition of shield to the system, sample 16 was prepared; thus, the only difference of these two samples is presence of shield during preparing this sample. AFM result of sample 16 illustrates partial monolayer coverage but small holes still exist on the surface (see Fig.4.21). This shows that, to obtain a complete coverage the best condition needs to be a little adjusted if working under the shield is preferred.

Sample 17, sample 18 and sample 19:

The next three experiments were conducted by mixing the orange QDs dissolved in chloroform with toluene solution. 3mL orange QDs dissolved in chloroform was added to 20 mL toluene. The experiment performed on $5mm \times 1cm$ RCA1 treated Si substrates at withdrawal speed of 0.1 mm/min and submersion time of 600s for sample 17 and 1200s for sample 18. AFM result for sample 17 and 18 are shown in Fig.4.22a and Fig. 4.22b,4.22d respectively. These results indicate that closed-packed QD layers with acceptable coverage is formed under this condition when longer submersion time is applied. Moreover, the patterens appeared in the phase AFM image of sample 18 (see Fig.4.22b) is exactly the same

on the top and bottom layer similar to what we earlier obsereved in phase image of sample 10 (see Fig.4.16dmiddle). Looks like the second layer is forming on the first layer. However to prove this observation, closer look on the sample by TEM is required. Sample 19 was prepared at condition the same as 18, but slower withdrawal speed of 0.05mm/min. The lower percentage monolayer coverage on this sample is another confirmation of optimum speed is about 0.1mm/min (see Fig.4.22c).

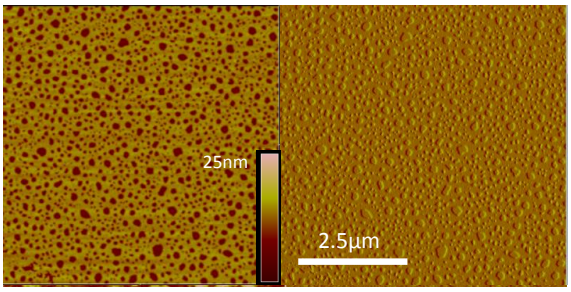

(a)

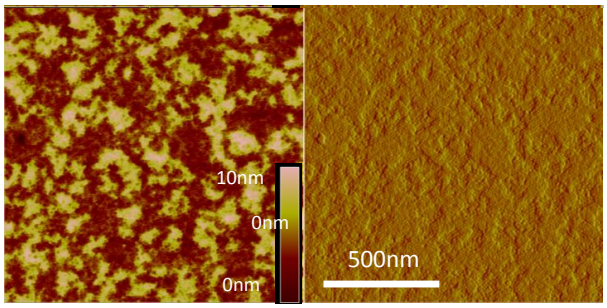

(b)

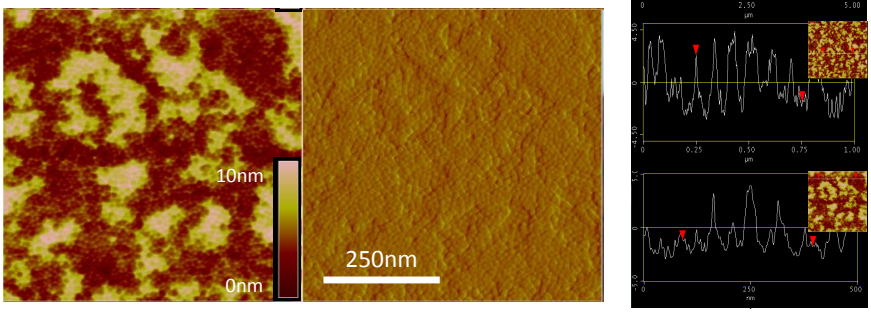

(c) (d)

Figure 4.16: Height (left) and corresponding phase (right) image of sample 10: 3 mL of yellow QDs injected in 20 mL of toluene, withdrawal speed of 0.1 mm/min and submersion time of 600s for a RCA1 treated $7mm \times 1cm$ silicon substrate a) scale bar=2.5m, b) scale bar=500nm and d) scale bar=250nm. The profile data along the white line (see insets) correspond to each height image.

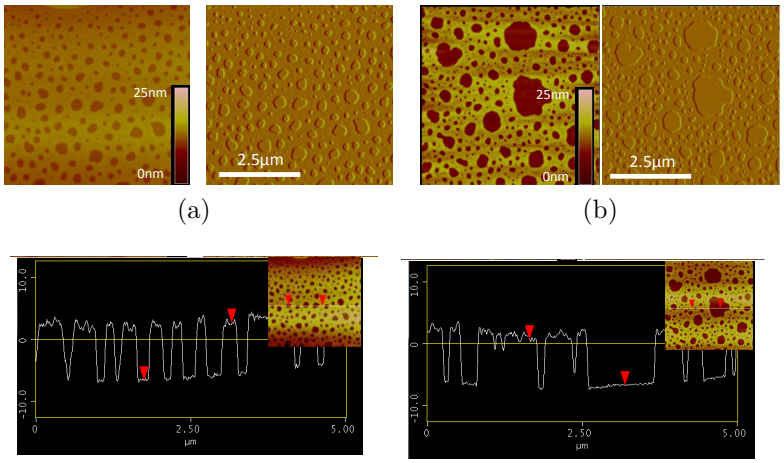

(a) (b)

(c) (d)

Figure 4.17: a,b) Height (left) and corresponding phase (right) image for different area of the sample 11: speed lowered to 0.05mm/min, c,d) corresponding profile data of a,b.

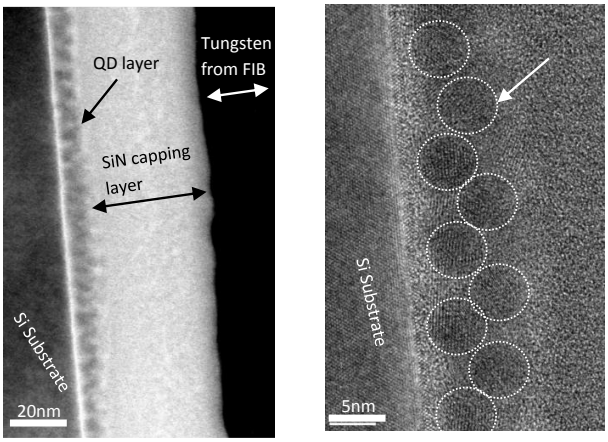

(a) (b)

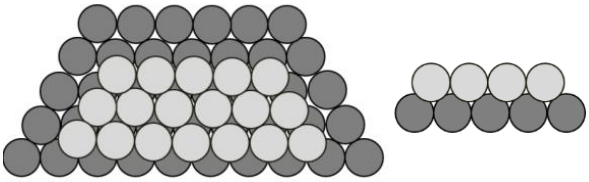

Hcp ordered QD layer/top view

Hcp ordered QD layer/cross section

(c)

Figure 4.18: a) TEM and b) HRTEM image of QD layer of sample 11. c) schematic illustration of hcp structure.

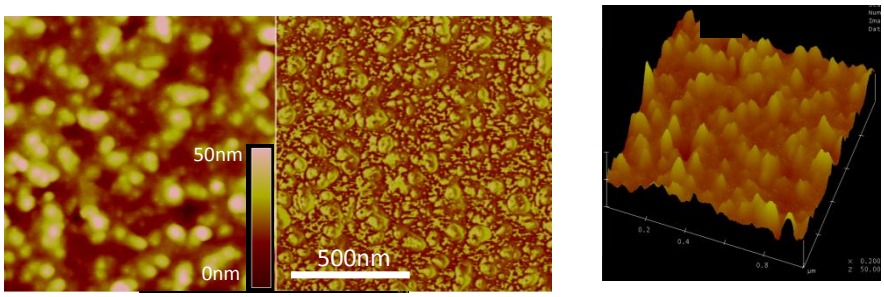

(a) (b)

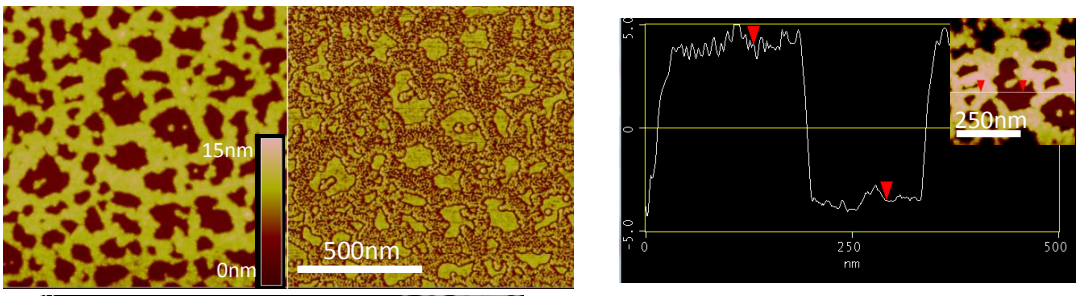

(c) (d)

Figure 4.19: a) Height (left) and corresponding phase (right) image of sample 12: QD layer formed on ZnO layer, b) 3D height AFM image extracted from (a), c) Height (left) and corresponding phase (right) image of sample 13: same condition applied on Si surface, d) Profile data of (c).

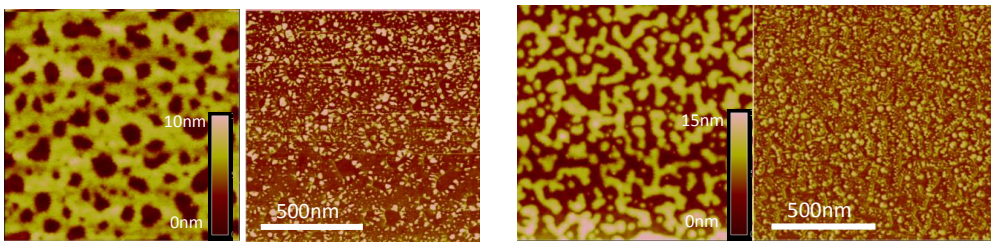

(a) (b)

Figure 4.20: Height (left) and corresponding phase (right) image of a) sample 14: QD layer formed on SiNx substrate and b) sample 15: QD layer formed on Si substrate.

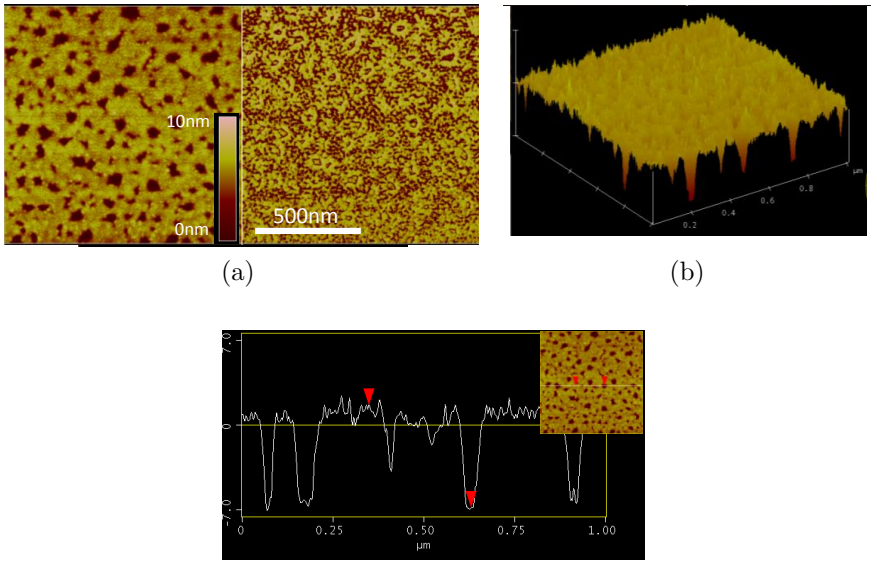

(a) (b)

(c)

Figure 4.21: a) Height (left) and corresponding phase (right) image of sample 16: layer formation under condition same as sample 10 when shield applied, b) 3D height AFM image extracted from (a), c) Profile data of (a)

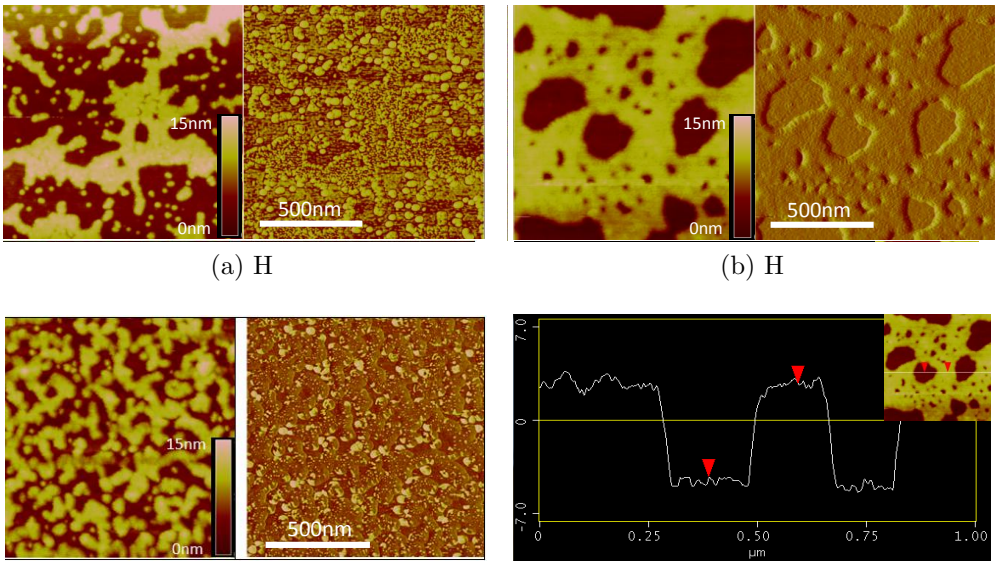

(a) H (b) H

(c) H (d) H

Figure 4.22: Height (left) and corresponding phase (right) image of a) sample 17: QDs dispersed in chloroform mixed with toluene / withdrawal speed of 0.1mm/min and submersion time of 600s , b) sample 18: submersion time of 1200s, c) sample 19: withdrawal speed of 0.1mm/min and submersion time of 1200s, d) AFM Profile data of (b).

4.4 Comparison With Earlier Simulation Results

Earlier simulations have been done to find energy band diagram for the ordered arrays of QDs grown by MBE method. In this chapter, the main goal is exploring the feasibility of growing ordered QDs layers using colloidal QDs. None-MBE methods for formation of QD superlattice structures in a controlled way are of great interest for research in this area due to the difficulties of MBE of QD. Colloidal QDs superlattice fabrication is an alternative approach for growing controlled self-assembled QD layers and is becoming an attractive research area due to its ease of deployment and cost efficient characteristic.

According to the simulation results shown in Fig. 4.23 QDs need to be perfectly ordered vertically for IB application. However, a 3D QD superlattice structure formed by colloidal QDs results in hexagonally closed packed (hcp) structure. As shown in Fig.4.24, in this type of structures QDs fill the gap between the two neighbouring QDs of the lower layer. To take into account this new QDs arrangement some modification to the model is required to be considered.

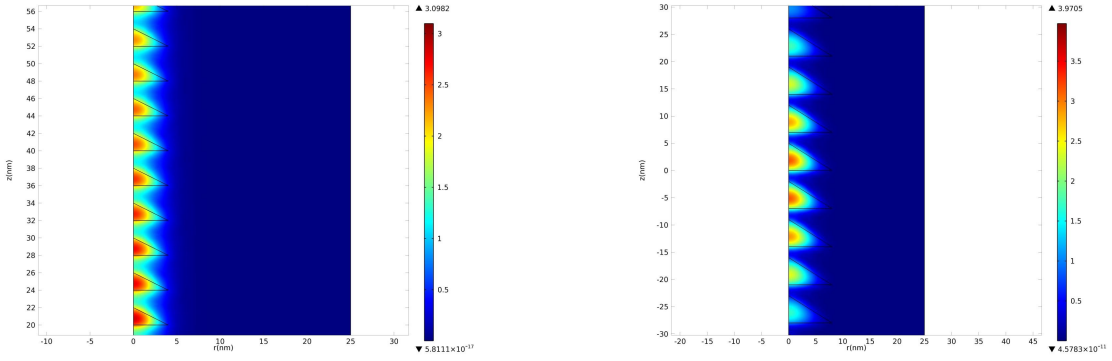

(a) (b)

Figure 4.23: Field distribution for (a) 60 conical QD of size1, energy level shown is 0.9862 ev (b)60 conical QD of size2, energy level shown is 0.4551 ev,(X axis: r(nm), Y axis: z(nm))

In order to converge this model with the theoretical study one possible approach would be embedding QDs in a matrix and growing the next layer on top of the capping material. Fig. 4.25 demonstrates a QD layer sandwiched between the substrate and silicon nitride

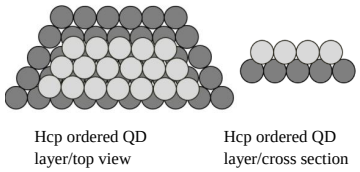

Figure 4.24: ordered monolayer of QDs capped with SiNx layer.

(SiNx) capping layer. Proper choice of capping material would result in similar and perfect ordering seen in the simulation.

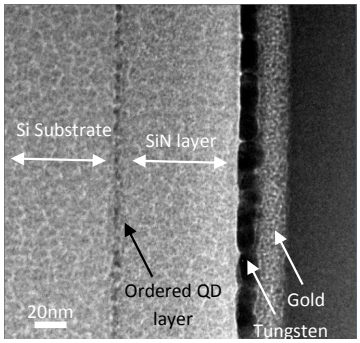

Figure 4.25: ordered monolayer of QDs capped with SiNx layer.

One key advantage of colloidal QDs over the MBE grown QDs is the absence of wetting layer in colloidal approach. In the simulation results obtained for the MBE grown QDs, it was observed that degrading effect of wetting layer on the band location was substantial. Removing the wetting layer would reduce one of the parasitic elements that blocks achieving the predicted high efficiency.

In the theoretical model QD sizes could be chosen arbitrarily to gain the optimized band location. On the other hand, in colloidal approach, there are some limitations on selecting the desired QD sizes due to the synthesized method used for formation of this type of QDs. Colloidal QDs are available in sizes ranging from 1.5 to 7.5nm. This causes the reduction of one degree of freedom in theoretical model. In order to have more realistic

results, it is required to pre-set the QD sizes in the simulation. The shape of QDs also needs to be changed from conical to spherical employing the cylindrical symmetry.

Chapter 5

Summery and Future Research

5.1 Summery

In this thesis basics of Intermediate Band Solar cell, its fabrication process and methods were reviewed. Different QDs used for IBSC fabrication were introduced. Effect of taking into account the realistic shape of QDs for band placing was examined via Comsol simulation. Simulation was conducted for different shapes, different number of vertically stacked QDs with addition of wetting layer or with its reduction. It was shown that the wetting layer disturbs three separate band formation. Effect of simplifying the quantum dot shape to a cubic one on band placing and the accuracy of this simplified simulation was explored.

In addition, the best condition for achieving self-assembled layer using colloidal QDs was studied. Formation of one or two layers of crystalline QDs layer has been investigated.the possibility of crystal formation for one or more than one layer has been confirmed. Also, possibility of embedding QD inside a matrix without damaging QDs has been shown. IB cells are currently fabricated via MBE method but,high expenses of fabrication process may eventually cause the cell fabrication to shift to cheaper for its mass production. one of attractive ways to realize this cost reduction could be use of colloidal QDs.

5.2 Future Work

It should be noted that IBSC although theoretically has been approved, has not been realized. Since many physical phenomena occur in the real device that have been discarded

in the theory and, they make many problems for device operation. For achieving the high promised efficiency all of these problems should be addressed. For example there should be some researches to find methods to suppress wetting layer formation during QD growth via MBE method due to deteriorating effect of wetting layer.

Other possible break through could be switching form MBE QD growth method which is an expensive and hard method to fast and cheap solution based QD self-assembly. Colloidal QDs have some characterises which are not suitable for IBSC such as low mobility and conductivity. Exchanging the organic ligand and doping would help to mitigate the negative sides of these QDs for IBSC. Also, another future work is to find ways to fabricate large number of stable stacked QD layers.

References

[1] Martin A. Green. *Third Generation Photovoltaics: Advanced Solar Energy*. springer, Verlog, Berlin, 2003.

[2] Antonio Luque and Antonio Martí. Increasing the efficiency of ideal solar cells by photon induced transitions at intermediate levels. *Phys. Rev. Lett.*, 78:5014–5017, Jun 1997.

[3] R. F. C. Farrow. *Molecular Beam Epitaxy*. William Andrew, Burlington, MA, 1995.

[4] C. B. Murray, D. J. Norris, and M. G. Bawendi. Synthesis and characterization of nearly monodisperse cde (e = sulfur, selenium, tellurium) semiconductor nanocrystallites. *Journal of the American Chemical Society*, 115(19):8706–8715, 1993.

[5] CB Murray, CR Kagan, and MG Bawendi. Synthesis and characterization of monodisperse nanocrystals and close-packed nanocrystal assemblies. *Annual Review of Materials Science*, 30(1):545–610, 2000.

[6] Martin A Green. Third generation photovoltaics: solar cells for 2020 and beyond. *Physica E: Low-dimensional Systems and Nanostructures*, 14(12):65 – 70, 2002.

[7] Martin A. Green, Keith Emery, Yoshihiro Hishikawa, Wilhelm Warta, and Ewan D. Dunlop. Solar cell efficiency tables (version 39). *Progress in Photovoltaics: Research and Applications*, 20(1):12–20, 2012.

[8] William Shockley and Hans J. Queisser. Detailed balance limit of efficiency of p-n junction solar cells. *Journal of Applied Physics*, 32(3):510–519, 1961.

[9] G.F. Brown and J. Wu. Third generation photovoltaics. *Laser and Photonics Reviews*, 3(4):394–405, 2009.

[10] H.A. Atwater and A. Polman. Plasmonics for improved photovoltaic devices. *Nature materials*, 9(3):205–213, 2010.

[11] Martin A Green. Third generation photovoltaics: solar cells for 2020 and beyond. *Physica E: Low-dimensional Systems and Nanostructures*, 14(12):65 – 70, 2002.

[12] M. Wolf. Limitations and possibilities for improvement of photovoltaic solar energy converters: Part i: Considerations for earth's surface operation. *Proceedings of the IRE*, 48(7):1246 –1263, july 1960.

[13] K. W. J. Barnham and G. Duggan. A new approach to high-efficiency multi-band-gap solar cells. *Journal of Applied Physics*, 67(7):3490–3493, 1990.

[14] Jenny Nelson, Ian Ballard, Keith Barnham, James P. Connolly, John S. Roberts, and Malcolm Pate. Effect of quantum well location on single quantum well p-i-n photodiode dark currents. *Journal of Applied Physics*, 86(10):5898–5905, 1999.

[15] F.W. Ragay, J.H. Wolter, A. Marti, and G.L. Araujo. Experimental analysis of gaas-ingaas mqw solar cells. In *Photovoltaic Energy Conversion, 1994., Conference Record of the Twenty Fourth. IEEE Photovoltaic Specialists Conference - 1994, 1994 IEEE First World Conference on*, volume 2, pages 1754 –1758 vol.2, dec 1994.

[16] A. Luque, A. Martí, and L. Cuadra. Thermodynamic consistency of sub-bandgap absorbing solar cell proposals. *Electron Devices, IEEE Transactions on*, 48(9):2118–2124, 2001.

[17] A. Luque, A. Marti, P. Wahnon, L. Cuadra, C. Tablero, C. Stanley, A. McKee, D. Zhou, R. Konenkamp, R. Bayon, A. Belaidi, J. Alonso, J. Ruiz, J. Fernandez, P. Palacios, and N. Lopez. Progress towards the practical implementation of the intermediate band solar cell. In *Photovoltaic Specialists Conference, 2002. Conference Record of the Twenty-Ninth IEEE*, pages 1190 – 1193, may 2002.

[18] A. Marti, L. Cuadra, and A. Luque. Partial filling of a quantum dot intermediate band for solar cells. *Electron Devices, IEEE Transactions on*, 48(10):2394 –2399, oct 2001.

[19] N. López, L. A. Reichertz, K. M. Yu, K. Campman, and W. Walukiewicz. Engineering the electronic band structure for multiband solar cells. *Phys. Rev. Lett.*, 106:028701, Jan 2011.

[20] L. Landin, M. S. Miller, M.-E. Pistol, C. E. Pryor, and L. Samuelson. Optical studies of individual inas quantum dots in gaas: Few-particle effects. *Science*, 280(5361):262–264, 1998.

[21] A. P. Alivisatos. Semiconductor clusters, nanocrystals, and quantum dots. *Science*, 271(5251):pp. 933–937, 1996.

[22] S. A. Empedocles and M. G. Bawendi. Quantum-confined stark effect in single cdse nanocrystallite quantum dots. *Science*, 278(5346):2114–2117, 1997.

[23] U. Gasser, Eric R. Weeks, Andrew Schofield, P. N. Pusey, and D. A. Weitz. Real-space imaging of nucleation and growth in colloidal crystallization. *Science*, 292(5515):258–262, 2001.

[24] D. J. W. Aastuen, N. A. Clark, L. K. Cotter, and Bruce J. Ackerson. Nucleation and growth of colloidal crystals. *Phys. Rev. Lett.*, 57:1733–1736, Oct 1986.

[25] Paul Harrison. *Quantum wells wires and dots*. John Wiley and Sons, Hoboken, New Jersey, 2009.

[26] D. L. Huffaker, G. Park, Z. Zou, O. B. Shchekin, and D. G. Deppe. 1.3 mu m room-temperature gaas-based quantum-dot laser. *Applied Physics Letters*, 73(18):2564–2566, 1998.

[27] S. Kim, H. Mohseni, M. Erdtmann, E. Michel, C. Jelen, and M. Razeghi. Growth and characterization of ingaas/ingap quantum dots for midinfrared photoconductive detector. *Applied Physics Letters*, 73(7):963–965, 1998.

[28] A.J Nozik. Quantum dot solar cells. *Physica E: Low-dimensional Systems and Nanostructures*, 14(12):115 – 120, 2002.

[29] Sungjee Kim, Brent Fisher, Hans-Jrgen Eisler, and Moungi Bawendi. Type-ii quantum dots: cdte/cdse(core/shell) and cdse/znte(core/shell) heterostructures. *Journal of the American Chemical Society*, 125(38):11466–11467, 2003. PMID: 13129327.

[30] Helmut Sitter Marian A. Herman. *Molecular Beam Epitaxy:: Fundamentals and Current Status*. Springer, London, UK, 1989.

[31] Y.-W. Mo, D. E. Savage, B. S. Swartzentruber, and M. G. Lagally. Kinetic pathway in stranski-krastanov growth of ge on si(001). *Phys. Rev. Lett.*, 65:1020–1023, Aug 1990.

[32] A. Luque, A. Marti, C. Stanley, N. Lopez, L. Cuadra, D. Zhou, J. L. Pearson, and A. McKee. General equivalent circuit for intermediate band devices: Potentials, currents and electroluminescence. *Journal of Applied Physics*, 96(1):903–909, 2004.

[33] R. B. Laghumavarapu, A. Moscho, A. Khoshakhlagh, M. El-Emawy, L. F. Lester, and D. L. Huffaker. Gasb/gaas type ii quantum dot solar cells for enhanced infrared spectral response. *Applied Physics Letters*, 90(17):173125, 2007.

[34] Voicu Popescu, Gabriel Bester, Mark C. Hanna, Andrew G. Norman, and Alex Zunger. Theoretical and experimental examination of the intermediate-band concept for strain-balanced (in,ga)as/ga(as,p) quantum dot solar cells. *Phys. Rev. B*, 78:205321, Nov 2008.

[35] A. Luque, A. Marti, E. Antolin, P. G. Linares, I. Tobias, and I. Ramiro. Radiative thermal escape in intermediate band solar cells. *AIP Advances*, 1(2):022125, 2011.

[36] C.H. Crouch, R. Mohr, T. Emmons, S. Wang, and M. Drndic. Excitation energy dependence of fluorescence intermittency in cdse/zns core-shell nanocrystals. *The journal of physical chemistry. C, Nanomaterials and interfaces*, 113(28):12059, 2009.

[37] CB Murray, CR Kagan, and MG Bawendi. Self-organization of cdse nanocrystallites into three-dimensional quantum dot superlattices. *Science*, 270(5240):1335–1338, 1995.

[38] J.M. Luther, M. Law, Q. Song, C.L. Perkins, M.C. Beard, and A.J. Nozik. Structural, optical, and electrical properties of self-assembled films of pbse nanocrystals treated with 1, 2-ethanedithiol. *Acs Nano*, 2(2):271–280, 2008.

[39] Andrea R. Tao, Jiaxing Huang, and Peidong Yang. Langmuirblodgettry of nanocrystals and nanowires. *Accounts of Chemical Research*, 41(12):1662–1673, 2008.

[40] A. Luque and A. Martí. The intermediate band solar cell: progress toward the realization of an attractive concept. *Advanced Materials*, 22(2):160–174, 2010.

[41] RVN Melnik and M. Willatzen. Bandstructures of conical quantum dots with wetting layers. *Nanotechnology*, 15(1):1, 2003.

[42] Q. Shao, A. A. Balandin, A. I. Fedoseyev, and M. Turowski. Intermediate-band solar cells based on quantum dot supracrystals. *Applied Physics Letters*, 91(16):163503, 2007.

[43] Hyunho Shin, Woong Lee, and Yo-Han Yoo. Comparison of strain fields in truncated and un-truncated quantum dots in stacked inas/gaas nanostructures with varying stacking periods. *Journal of Physics: Condensed Matter*, 15(22):3689, 2003.

[44] M.Y. Levy, C. Honsberg, A. Marti, and A. Luque. Quantum dot intermediate band solar cell material systems with negligible valence band offsets. In *Photovoltaic Specialists Conference, 2005. Conference Record of the Thirty-first IEEE*, pages 90 – 93, jan. 2005.

[45] A. Marti, N. Lopez, E. Antolin, E. Canovas, A. Luque, C. R. Stanley, C. D. Farmer, and P. Diaz. Emitter degradation in quantum dot intermediate band solar cells. *Applied Physics Letters*, 90(23):233510 –233510–3, jun 2007.

[46] Olga L. Lazarenkova and Alexander A. Balandin. Electron and phonon energy spectra in a three-dimensional regimented quantum dot superlattice. *Phys. Rev. B*, 66:245319, Dec 2002.

[47] Olga L. Lazarenkova and Alexander A. Balandin. Miniband formation in a quantum dot crystal. *Journal of Applied Physics*, 89(10):5509 –5515, may 2001.

[48] Dip-coating. http://www.ytca.com/dip_coating, 2013. [Online; accessed January-2013].